Confined Lateral Diffusion of Membrane Receptors as Studied by Single Particle Tracking (Nanovid Microscopy). Effects of Calcium-Induced Differentiation in Cultured Epithelial Cells

Akihiro Kusumi, Yasushi Sako, and Mutsuya Yamamoto

Department of Pure and Applied Sciences, The University of Tokyo, Meguro-ku, Tokyo 153, Japan

ABSTRACT   The movements of E-cadherin, epidermal growth factor receptor, and transferrin receptor in the plasma membrane of a cultured mouse keratinocyte cell line were studied using both single particle tracking (SPT; nanovid microscopy) and fluorescence photobleaching recovery (FPR). In the SPT technique, the receptor molecules are labeled with 40 nm-ϕ colloidal gold particles, and their movements are followed by video-enhanced differential interference contrast microscopy at a temporal resolution of 33 ms and at a nanometer-level spatial precision. The trajectories of the receptor molecules obtained by SPT were analyzed by developing a method that is based on the plot of the mean-square displacement against time. Four characteristic types of motion were observed: (a) stationary mode, in which the microscopic diffusion coefficient is less than 4.6×10^{-12} cm^2/s; (b) simple Brownian diffusion mode; (c) directed diffusion mode, in which unidirectional movements are superimposed on random motion; and (d) confined diffusion mode, in which particles undergoing Brownian diffusion (microscopic diffusion coefficient between 4.6×10^{-12} and 1×10^{-9} cm^2/s) are confined within a limited area, probably by the membrane-associated cytoskeleton network. Comparison of these data obtained by SPT with those obtained by FPR suggests that the plasma membrane is compartmentalized into many small domains 300–600 nm in diameter (0.04–0.24 μm^2 in area), in which receptor molecules are confined in the time scale of 3–30 s, and that the long-range diffusion observed by FPR can occur by successive movements of the receptors to adjacent compartments. Calcium-induced differentiation decreases the sum of the percentages of molecules in the directed diffusion and the stationary modes outside of the cell-cell contact regions on the cell surface (which is proposed to be the percentage of E-cadherin bound to the cytoskeleton/membrane-skeleton), from ~60% to 8% (low- and high-calcium mediums, respectively).

INTRODUCTION

Cells regulate the localization, assembly, and molecular aggregation state of many integral membrane proteins in the plasma membrane, ensuring the proper functions of these proteins. Special membrane domains such as coated pits (Goldstein et al., 1985), cell-cell adhesion structures (Kusumi et al., 1990), and synaptic junctions (Dubinsky et al., 1989) are formed by the assembly of specific proteins to carry out specific functions. Association of ligand-receptor complexes has been proposed to be a critical step for triggering the cellular responses by many receptors such as immunoglobulin E-Fc receptors (Metzger's review, 1992) and epidermal growth factor (EGF) receptors (Schlessinger, 1986). Since such processes take advantage of the lateral mobility of integral membrane proteins, understanding these processes requires detailed knowledge regarding the movements of membrane proteins and their control mechanisms in the plasma membrane. In addition, observation of protein mobility in the plasma membrane can provide valuable information on interactions between membrane constituent molecules (Cherry, 1979; Kusumi and Hyde, 1982; Edidin, 1987, 1990; Saxton, 1987, 1989a, b, 1990, 1992; Abney et al., 1989; Ghosh and Webb, 1990; Edidin and Stroynowski, 1991; Edidin et al., 1991; Zhang et al., 1991;

De Brabander et al., 1991), particularly between integral membrane proteins and the membrane-associated cytoskeleton (membrane skeleton network) (Sheetz et al., 1980; Tsuji et al., 1988).

To monitor the dynamics of membrane proteins, fluorescence photobleaching recovery (FPR) has been used to observe lateral diffusion (Axelrod et al., 1976; Jacobson et al., 1987), while anisotropic decay of triplet probes (Cherry et al., 1976; Austin et al., 1979; Moore et al., 1979; Tsuji et al., 1988; Johnson and Garland, 1981; Zidovetzki, 1986) and saturation transfer ESR spectroscopy (Hyde and Dalton, 1972; Thomas et al., 1976; Kusumi et al., 1978, 1980; Kusumi and Hyde, 1982) have been used to observe rotational diffusion. For example, investigations of the interaction between band 3 and the spectrin network in human erythrocytes were carried out using both lateral and rotational diffusion measurements of band 3 (Tsuji and Ohnishi, 1986; Tsuji et al., 1988). By observing the rotational diffusion of band 3, it was found that the immobile fraction of band 3 in lateral diffusion measurements using FPR (~20% at 37°C) is due to the binding of band 3 to the spectrin network, rather than to the trapping of band 3 in the spectrin meshwork, and that the effect of the meshwork on the mobile fraction of band 3 is to decrease the diffusion coefficient by a factor of 10. Since the spatial resolution of FPR is in the range of 1 μm, rotational diffusion measurement is often required for obtaining information at the nanometer or molecular levels. Such complementary measurements of band 3 diffusion under conditions that varied spectrin's dimer-tetramer equilibrium

led Tsuji and co-workers to propose a spectrin dimer/ tetramer equilibrium gate model (SPEQ gate model) (Tsuji and Ohnishi, 1986; Tsuji et al., 1988); that is, the immobile fraction of band 3 at 37°C (~20%) is due to the binding of band 3 to the spectrin network and is not due to the fence effect of the spectrin network, whereas the rate of macroscopic diffusion of the mobile fraction of band 3 is determined by the frequency at which band 3 passes the spectrin fence, which depends on the equilibrium between spectrin dimers (open gate or broken fence) and tetramers (closed gate or intact fence) (hence the name "SPEQ gate model").

A new method has recently been developed for tracking the movements of single nanometer-size particles under an optical microscope (nanovid microscopy) (De Brabander et al., 1985, 1986, 1988; Geerts et al., 1987, 1991) with the possibility of nanometer-level precision (Gelles et al., 1988; Schnapp et al., 1988; Sheetz et al., 1989). Qian et al. (1991) presented the theoretical basis for analyzing trajectories obtained by single particle tracking (SPT) with an emphasis on random diffusion and systematic transport at a uniform velocity. Saxton (1993) described the probabilities of occurrence of various trajectories. The SPT method is unique in that it can reveal the mechanisms that are working on a single (or a few) protein molecule(s) in the plasma membrane for regulating its (their) motion. In addition, the nanometer-level precision of SPT is particularly useful for studying molecular mechanisms working at the submicron scale, such as in the spectrin network. As mentioned above, both lateral and rotational diffusion measurements were previously needed to obtain information at the nanometer or molecular level. Another approach similar to SPT using fluorescence microscopy is now available to characterize movements of fluorescently labeled receptors, but with lower spatial and temporal resolutions (Gross and Webb, 1988; Ghosh and Webb, 1990; Anderson et al., 1992; Cherry, 1992).

The aim of this work is fivefold: (a) to compare SPT and FPR data to examine the validity of the newly-developed SPT technique; (b) to obtain information on the membrane structure at a nanometer-micrometer scale by comparing SPT and FPR data; (c) to develop methods for classifying the observed trajectories of SPT into the four types of motion that are believed to occur in the plasma membrane (stationary mode, simple Brownian diffusion mode, directed diffusion mode, and restricted diffusion mode, in which a particle undergoing free diffusion is confined within a limited area); (d) to investigate the mechanisms that regulate the movements of E-cadherin, epidermal growth factor receptor (EGF-R), and transferrin receptor (Tf-R) in both undifferentiated and differentiated states of mouse keratinocytes in culture; and (e) to examine the membrane domain structure as it is "felt" by the receptor molecules and to test the "membrane skeleton fence model" (Tsuji et al., 1988).

The membrane skeleton fence model proposes that the membrane-associated cytoskeleton meshwork (membrane skeleton) provides a barrier to free diffusion of membrane proteins via steric hindrance (the space between the membrane and the cytoskeleton is too small to allow the cytoplasmic portion of the membrane protein to pass), thus com-

partmentalizing the membrane into many small domains (the mesh size of which is 300–600 nm in diameter, as we have determined in the present work). The membrane proteins can escape from one domain and move to adjacent compartments because of the dynamic properties of the membrane skeleton; the distance between the membrane and the skeleton may fluctuate over time, thus giving the membrane proteins an opportunity to pass through the mesh barrier, the membrane skeleton may dissociate from the membrane, and the membrane-skeleton network may form and break continuously due to dissociation-association equilibrium of the cytoskeleton. The SPEQ gate structure is a specific case of the membrane skeleton fence model in human erythrocyte membrane. Saxton (1990, 1991) quantitatively evaluated the long-range behavior of membrane proteins in the membrane skeleton fence meshwork.

We will pay special attention to the differences in the movements of E-cadherin, a cell-cell recognition-adhesion receptor, before and after Ca^{2+}-induced differentiation of a mouse keratinocyte cell line (F7p) (Hennings et al., 1980). E-cadherin plays important roles in tissue morphogenesis (Takeichi, 1988). When F7p cells are cultured in a medium containing normal Ca^{2+} concentrations (1.4 mM, high-calcium medium), the cells are stratified, mimicking the differentiation pathway in the normal skin tissue. The cells adhere strongly to each other via E-cadherin and desmosomes. Although many cadherin molecules are spread over the entire cell surface, most cadherin molecules are assembled at the cell-cell boundary. When the cells are cultured in a low-calcium medium containing 50 μM Ca^{2+}, cell-cell adhesion is lost, desmosomes are cleared from cell surfaces, E-cadherin is homogeneously spread over cell surfaces, and the cells remain in an undifferentiated state. Cell-cell adhesion and differentiation of the cells cultured in the low-calcium medium can be induced just by raising the Ca^{2+} concentration of the medium to above 0.3 mM (calcium switch). On the other hand, dedifferentiation and dissociation of cells cultured in a high-calcium medium can be induced by lowering the Ca^{2+} concentration in the medium to 30–50 μM (Hennings et al., 1980, 1989). Therefore, the calcium switch of a keratinocyte cell line in culture provides a convenient model with which to study changes in the regulation of E-cadherin movements and assembly in undifferentiated and differentiated cells. In the present study, only cadherin molecules on cell surfaces outside of the cell-cell boundary regions were examined to study the mechanism that regulates cadherin movements (to the boundary regions). To determine whether or not the changes are specific to E-cadherin, movements of EGF-R and Tf-R were also studied under both high- and low-calcium conditions. Comparison with FPR data and development of the method for classification of the motional modes were carried out using E-cadherin as a model system.

MATERIALS AND METHODS

Cell cultures

1981; Kulesz-Martin et al., 1983) at the U.S. National Cancer Institute. The cells were routinely cultured in a minimum essential medium at a normal calcium concentration (~1.4 mM, Hi-MEM (minimum essential medium), Earle's salt) supplemented with nonessential amino acids, 10% fetal bovine serum, and a reduced concentration of $NaHCO_3$ (0.45 g/liter to lower the pH of the medium) in a 5% CO_2 atmosphere at 36.5°C. The growth rate was comparable to that attained with the published culture conditions of 1 g/liter under 7% CO_2 atmosphere at 36°C (Hennings et al., 1980). For studies in a low-calcium medium, the cells were cultured in MEM containing ~50 μM Ca^{2+} (Lo-MEM) for 48 h. The calcium concentration in the medium was measured by atomic absorption spectroscopy after the medium was hydrolyzed with acid. Cells used for microscopic observation were cultured on 18 mm × 18 mm coverslips (no. 1).

Preparation of gold particles for labeling membrane proteins

Gold particles (40 nm in diameter) were prepared as described previously (de Mey, 1983; Leunissen and De Mey, 1986). Anti-E-cadherin monoclonal antibody (ECCD-2) (the hybridoma line is a gift from Dr. Takeichi at Kyoto University) was coupled to the gold particles by mixing the gold suspension and 0.4 mg/ml of antibody in 67 mM phosphate buffer at pH 7.4 at a ratio of 1:1. After incubation at 4°C for 1 h, the labeled gold particles were stabilized by further addition of bovine serum albumin (BSA) in 67 mM phosphate buffer at a final concentration of 1% (w/v).

To label receptors for transferrin and mouse epidermal growth factor (EGF), these ligands were bound to the gold particles via BSA by using a cross-linker (Yoshitake et al., 1982). First, BSA was attached to gold particles as described above at pH 6.0. Unbound BSA was removed by repeated centrifugation and resuspension of gold particles. Transferrin (2.0 mg) (Wako, Tokyo) or EGF (0.4 mg) (HIH, Tokyo) dissolved in 0.3 ml of phosphate buffer (67 mM, pH 7.0) was incubated with 1.6 mg of N-(ϵ-maleimidecaproyloxy)succinimide (EMCS) (Dojin, Kumamoto, Japan) at 30°C for 1 h. Unreacted EMCS was removed by gel filtration using Sephadex G-25 (Pharmacia). The EMCS-bound proteins and BSA-coated gold particles were mixed and incubated at 4°C for 24 h.

Gold particles that were complexed with either the antibody or the ligands were washed by repeated centrifugation and resuspension in 67 mM phosphate buffer at pH 7.0 and finally resuspended in Lo-MEM containing 5 mM piperazine-N,N'-bis(2-ethanesulfonic acid). For experiments involving Hi-MEM, the final calcium concentration was adjusted to 1.4 mM by adding 1.0 M $CaCl_2$.

Video microscopy

Living cells were labeled with the antibody- or ligand-bound gold particles. MEM solution of gold particles (~1 nM of gold particles, 60 μl) was added to the cells on a coverslip and incubated for 20 min at 36.5°C to label E-cadherin and at 4°C to label Tf-R and EGF-R. Preparations for microscopy were made by inverting the coverslip with the cells on a microscope slide glass using strips of adhesive tape (~0.2 mm thick) as spacers. The microchamber was either sealed with paraffin or perfused manually. The video-enhanced contrast microscopy and analysis system used for this study is illustrated in Fig. 1. A Zeiss Axioplan microscope was equipped with a condenser lens (numerical aperture = 1.4) and a 100× Plan-Neofluar objective (numerical aperture = 1.3). The sample was maintained at a temperature of 36.5 ± 1°C by covering the microscope with a specially designed plastic chamber and using a Nikon temperature controller (model NP-2). Cells were observed by video-enhanced differential interference contrast microscopy, with illumination through an optical fiber (Technical Video, Woods Hole, MA) by using the green line (wavelength = 546 nm) of a 100-W mercury arc lamp (HBO100). The image was projected on a Hamamatsu CCD camera (C2400-77; Hamamatsu, Japan). Real-time mottle subtraction and contrast enhancement were achieved with a Hamamatsu DVS-3000 image processor, and the processed image was recorded on a Panasonic TQ-3100F laser disk recorder.
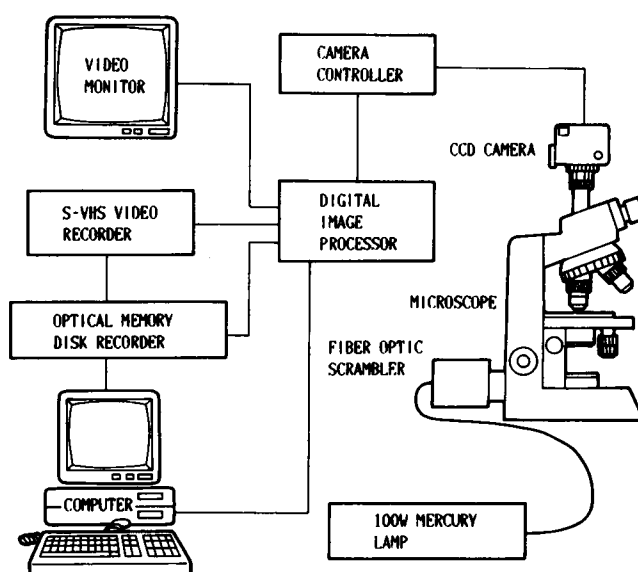

FIGURE 1   Block diagram of the instrument used for single particle tracking (nanovid microscopy). See the text for details.

Quantitative measurements of the movements of colloidal gold particles

The video images were digitized with a DVS-3000, and selected areas of the image were sent to a computer (Epson 286VF equipped with a Canoupus MC68020 add-on CPU board; Kobe, Japan). Positions (x and y coordinates) of selected gold particles were determined automatically with a computer by using a method developed by Gelles et al. (1988). The accuracy of the position measurement was estimated by recording a sequence of 150 video frames of the images of a 40-nm gold particle fixed on a polylysine-coated coverslip and impregnated in 10% polyacrylamide gel. The SDs of the measured coordinates of the fixed particles were 1.8 nm horizontally and 1.4 nm vertically, which were comparable to the published values (0.5–1 nm for 190-nm latex particles; Gelles et al., 1988; Schnapp et al., 1988). The nominal diffusion coefficient of the fixed particle was 3.2 × 10^{-13} cm^2/s, which therefore was the lower limit for determining the diffusion coefficient with the present settings.

FPR measurements of E-cadherin mobility

FPR measurements of E-cadherin on the cell surface (excluding the cell-cell contact regions) were carried out essentially as described by Tsuji and Ohnishi (1986), using an instrument in Dr. Ohnishi's laboratory at Kyoto University (Chang et al., 1981; Kusumi et al., 1986). The size of the bleached and observed area was 0.9 μm, with a typical observation time of 400 s. The temperature of the sample and the microscope was maintained at 36.5 ± 1°C. E-cadherin on the cell surface was labeled by incubating the living cells on the coverslip in MEM containing 0.04 mg/ml fluorescein-conjugated anti-E-cadherin rat monoclonal antibody (ECCD-2) and 2 mM piperazine-N,N'-bis(2-ethanesulfonic acid) at 4°C for 45 min. After washing out unbound antibodies, cells were used for FPR measurements. No internalization of the antibody-cadherin complex was observed at 36.5°C for at least 4 h.

RESULTS

Experimental observations

Characterization of E-cadherin mobility by the FPR method

We first characterized the mobility of E-cadherin on the cell surface using the FPR technique. This method has been used since 1976 (Axelrod et al., 1976; Elson, 1985) and would

provide a basis for evaluating the SPT results. Since we are interested in the mechanisms that control the movements of cadherin in the plasma membrane, we only studied the movements of E-cadherin and other receptors outside of the cell-cell boundary regions on the dorsal cell surface.

For FPR measurements, living cells were labeled from outside of the cell by adding fluorescein-labeled anti-E-cadherin monoclonal antibody, ECCD-2 (ECCD-2 does not inhibit cell adhesion). Strong localization of E-cadherin at the cell-cell boundaries, as well as weaker, uniform staining throughout the cell surface, was observed in the high-calcium medium. In the low-calcium medium, little cell-to-cell attachment was found and E-cadherin was spread uniformly over the entire cell surface (data not shown) (Kusumi et al., 1990, 1992; McNeill et al., 1990).

The results of the FPR measurements are summarized in Table 1. The results of SPT, also listed in Table 1, are shown for comparison with the FPR data and are discussed later. The data show that approximately one-third of the E-cadherin molecules are immobile in a time scale of 400 s and a space scale of ~0.9 μm in both high- and low-calcium mediums. The diffusion coefficients for the mobile fractions, which represent two-thirds of the E-cadherin molecules under either calcium condition, are small, that is, 2.6 and 3.4 $\times$ 10^{-11} cm^2/s in low- and high-calcium mediums, respectively. In summary, FPR data suggest that there are only slight differences in the mobility of E-cadherin under high- and low-calcium conditions.

These FPR data provide a basis for analyzing the SPT data. Furthermore, by comparing the SPT and FPR data, important features of the plasma membrane (i.e., the domain structure of the membrane) can be studied. SPT is sensitive to structural features in the submicrometer regime, while FPR is sensitive to membrane structure in the micrometer regime. Therefore, a variety of models for membrane structure and

the dynamics of membrane proteins can be examined in detail, because they must be consistent with both FPR and SPT data.

Trajectories of gold particles attached to E-cadherin

Gold particles attached to E-cadherin via ECCD-2 were distributed throughout the cell surface, as was observed by immunofluorescence staining, which was uniformly distributed over the cell surface in both high- and low-calcium mediums and concentrated at the cell-cell boundary in the high-calcium medium. A video-enhanced contrast image of mouse keratinocytes (F7p) labeled with gold particles via anti-E-cadherin monoclonal antibody in Hi-MEM is shown in Fig. 2. The gold particles coated only with BSA did not bind to the cells (here and later in this section, "no binding" indicates that the level of binding was less than 5% of that for the control experiment). No binding of ECCD-2-gold particles was observed when the cells were incubated with these particles in the presence of a 100-fold excess (over the number of gold particles) of ECCD-2.

To further examine the specific binding of ECCD-2-gold particles, mouse fibroblastic L cells, which do not express detectable amounts of E-cadherin, and a line of transfected L cells with E-cadherin complementary DNA (ELβ1a) (Nagafuchi and Takeichi, 1988) were used. Gold particles conjugated with anti-E-cadherin antibody attached to ELβ1a, but not to L cells, and gold particles conjugated with only BSA did not bind to either type of cell (data not shown).

To test the possibility of multivalent binding of gold particles to the receptor molecules and its effects on the observed motion, the size of the gold particles was varied (10, 20, 30, and 40 nm in diameter). Although it is difficult to differentiate between smaller gold particles on the cell surface and intracellular vesicles, it can be done if thin lamellapodial portions of the cells are observed. No difference was ob-

TABLE 1   FPR measurements of E-cadherin mobility, showing the fractions (%) of mobile and immobile components of E-cadherin and the (macroscopic) diffusion coefficients (x10⁻¹¹ cm²/s) for the mobile component at 36.5°C, and summary of the results of SPT

Ca^{2+} concentration	Mobile fraction (%)		Macroscopic diffusion coefficient of the mobile fraction ($\times$10^{-11} cm^2/s)		
	FPR*	SPT‡	FPR	SPT§ (macro)	SPT¶ (micro)
Low (50 μM)	75	78	2.6 $\pm$ 1.1	1.4	3.3 $\pm$ 2.9
High (1.4 mM)	64	94	3.4 $\pm$ 2.0	1.6	6.2 $\pm$ 7.6

* Estimated error is within $\pm$8%.

‡ Percentages of particles excepting the stationary mode as determined by the SPT technique. Details will be given later in the text.

§ Obtained by taking an ensemble average of SPT particles during 30 s (excluding particles in the stationary mode).

¶ The microscopic diffusion coefficient as determined by SPT in the simple and the restricted diffusion modes. For the difference between the macroscopic and microscopic diffusion coefficients, see the subsection Comparison with FPR results at the end of the Results section.
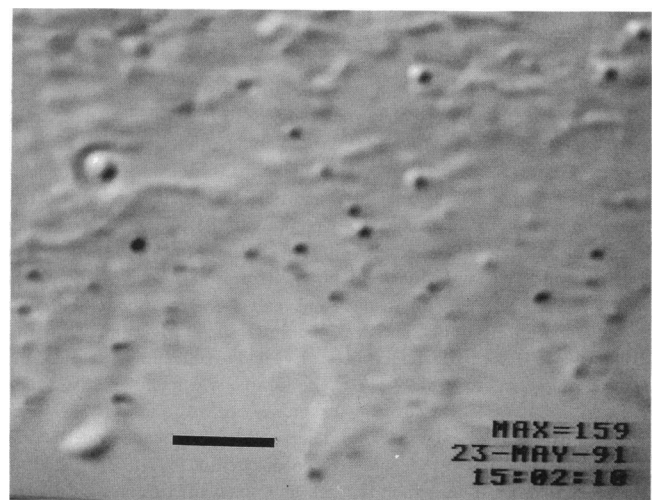

FIGURE 2   A video-enhanced differential interference contrast image of the cultured mouse keratinocyte cells labeled with gold particles that are complexed with anti E-cadherin monoclonal antibody (ECCD-2). The bar indicates 3 μm.

served with regard to the trajectories of the gold particles and the diffusion coefficients. We chose to use 40-nm gold particles for this study because they are easier to observe throughout the cell surface because of the higher contrast (the extent of light scattering is proportional to the sixth power of the diameter in this size domain) (Schnapp et al., 1988). Observation of the gold-labeled cells by transmission electron microscopy using the method of Miller et al. (1991) revealed that most of the gold particles (98%) were single particles (not aggregated).

The off-rates of ECCD-2 and its complex with gold particles from cadherin on the cell surface were rather low. When the cells were first incubated with ECCD-2 and then, after washing out the unbound ECCD-2, incubated with the ECCD-2-gold particles, no binding of gold particles to the cells was observed (the number of added gold particles per cell is 1–4 × 10⁵, which may be comparable to the number of cadherin molecules on the cell surface). When the cells were prelabeled with either ECCD-2-gold particles or fluorescein-conjugated ECCD-2, the extent of labeling did not decrease for at least 4 h in either the presence or absence of excess amounts of ECCD-2 in the incubating medium.

Typical trajectories of the movements of E-cadherin are shown in Fig. 3, A–D, and those of EGF-R and Tf-R are shown in Fig. 3, E and F, respectively. In these representations of trajectories, the positions of a particle, as determined frame by frame in a video sequence, are connected by straight lines. The trajectories are complex, and comparison with the trajectories of simple Brownian diffusion generated by computer simulation suggested that many trajectories could not be analyzed by free random diffusion. Therefore, we have developed the following method to analyze these data. Readers who are not interested in the technical aspect are recommended to move to the section "Characteristics of receptor movements" above Fig. 9.
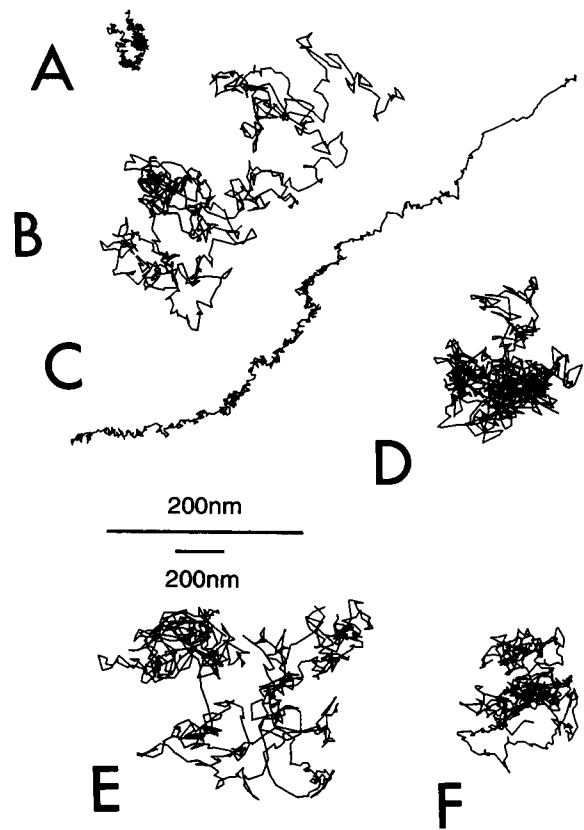

FIGURE 3 Typical trajectories of gold particles attached to E-cadherin (A–D), EGF-R (E), and Tf-R (F) on the cell surface for 30 s (900 steps) at 36.5°C. The MSD-Δt plots for B, C, and D are shown in Figs. 4 B, C, and D, respectively. According to the classification based on the MSD-Δt plot, (A) stationary mode ($D_{2–4}$ = 0.11 × 10⁻¹¹ cm²/s); (B) simple diffusion mode; (C) directed diffusion mode; (D) restricted diffusion mode; (E) EGF-R, simple diffusion mode; (F) Tf-R, simple diffusion mode. The bar indicates 200 nm.

Development of methods of SPT data analysis

Five models for the movements of membrane proteins

For each trajectory of a particle, the two-dimensional mean square displacement (MSD), $(\Delta r(\Delta t))^2$, for every time interval was calculated according to the formula (Gross and Webb, 1988; Lee et al., 1991; Qian et al., 1991):

$$\text{MSD}(\Delta t_n) = \text{MSD}(n\delta t) = \text{MSD}_x(n\delta t) + \text{MSD}_y(n\delta t) \quad (1)$$

$$= \frac{1}{N-1-n} \sum_{j=1}^{N-1-n} \{[x(j\delta t + n\delta t) - x(j\delta t)]^2$$

$$+ [y(j\delta t + n\delta t) - y(j\delta t)]^2\} \quad (2)$$

$$\Delta t_n = n\delta t \quad (3)$$

$$\delta t = 0.033 \text{ s (video frame time)} \quad (4)$$

where $(x(j\delta t + n\delta t), y(j\delta t + n\delta t))$ describes the particle position following a time interval $\Delta t_n = n\delta t$ after starting at position $(x(j\delta t), y(j\delta t))$, N is the total number of frames in the video recording sequence, and n and j are positive integers, with n determining the time increment. Eq. 1 simply shows that the two-dimensional MSD is the sum of the MSDs in the x and y directions.

Anisotropy in the protein movements in the plane of the membrane (such as unidirectional drift motion caused by drag of the cytoskeleton or lipid flow in the membrane) was evaluated as follows: by applying a least-square analysis to the N positions in a two-dimensional plane determined from a sequence of N video frames, the best-fit linear line was determined and labeled as the x-axis (parallel to the direction of transport). The y-axis was set perpendicular to the x-axis.

Five modes of motion are considered in order to describe the motional behavior of integral membrane proteins in the plasma membrane. These motional modes can be characterized on the basis of the plot of MSD versus time intervals (Fig. 4). In the present work, movements over a period of 3 s (n = 90) out of a video sequence of 33.3 s (N = 1000) were the primary focus of analysis.

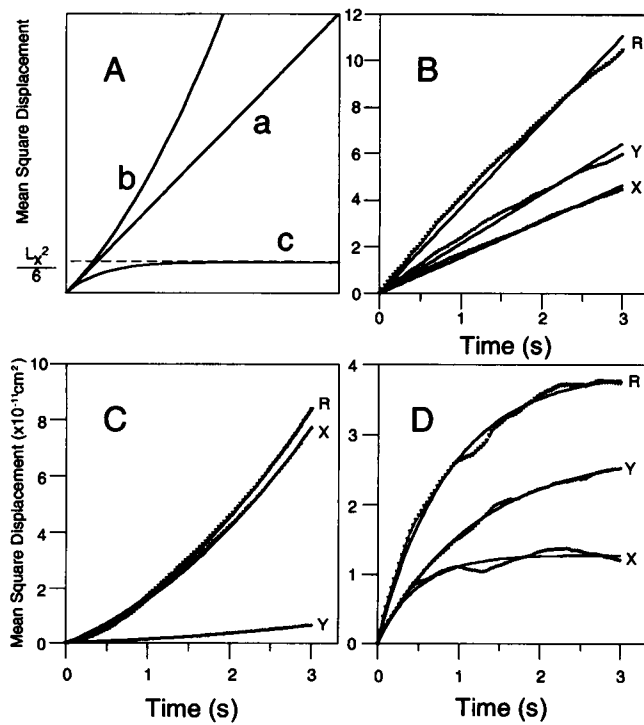1. *Stationary mode*, in which protein molecules show little motion. As will be discussed below, gold particles

FIGURE 4   MSD-Δt plots for diffusing particles. (A) theoretical curves for simple Brownian diffusion (a, mode 2, Eq. 5), directed diffusion (b, mode 3, Eq. 8), and restricted diffusion (c, mode 4, Eq. 11) are shown for one-dimensional diffusion (x direction). The graphs are drawn assuming that values for D are identical for all cases (the slope at time 0 is $2D$). (B and D) typical MSD-Δt plots for simple diffusion (B; $D = 0.92 \times 10^{-11}$ cm^2/s), directed diffusion (C; $D = 0.30 \times 10^{-11}$ cm^2/s, $v_x = 22$ nm/s, $v_y = 6$ nm/s), and restricted diffusion (D; $D = 1.35 \times 10^{-11}$ cm^2/s, $L_x = 88$ nm, $L_y = 128$ nm). X, Y, and R indicate diffusion in the x and y directions and in a two-dimensional plane, respectively. These plots are obtained from the trajectories of E-cadherin shown in Fig. 3, B, C, and D, respectively.

that show $D_{2-4} < 4.6 \times 10^{-12}$ cm^2/s are classified in this category in the present research (D_{2-4} is defined in the next subsection).

2. *Simple diffusion mode*, in which protein molecules undergo simple Brownian diffusion. In this case, the MSD-Δt plot (Fig. 4, A-a and B) is linear with a slope of $4D$, and can be expressed as

$$\text{MSD}_x(\Delta t) = 2D_x \Delta t, \qquad \text{MSD}_y(\Delta t) = 2D_y \Delta t \qquad (5)$$

$$\text{MSD}(\Delta t) = 4D\Delta t \qquad (6)$$

$$4D = 2D_x + 2D_y \qquad (7)$$

where D is the two-dimensional diffusion coefficient and D_x and D_y are one-dimensional diffusion coefficients for the x and y directions, respectively.

Fig. 3 B shows a typical trajectory of a particle undergoing simple Brownian diffusion, and the corresponding MSD-Δt plot is shown in Fig. 4 B. The MSD increases linearly with the time interval, and a diffusion coefficient of 0.92×10^{-11} cm^2/s was obtained from the slope.

3. *Directed diffusion mode (transport mode)*, in which a protein molecule moves in a direction at a constant drift velocity v_x (v_y), with superimposed random diffusion with a diffusion coefficient D_x (D_y). The MSD-Δt plot (Fig. 4, A-b and C) is parabolic with a differential coefficient of $4D$ at time 0 (initial slope).

$$\text{MSD}_x(\Delta t) = 2D_x\Delta t + v_x^2(\Delta t)^2, \qquad (8)$$
$$\text{MSD}_y(\Delta t) = 2D_y\Delta t + v_y^2(\Delta t)^2$$

$$\text{MSD}(\Delta t) = 4D\Delta t + v^2(\Delta t)^2 \qquad (9)$$

$$v^2 = v_x^2 + v_y^2. \qquad (10)$$

Fig. 3 C shows a typical trajectory of a particle exhibiting unidirectional motion in the x direction (based on the above definition of the x direction), upon which small random motions in both the x and y directions are superimposed. Thus, the MSD-Δt plot gives a parabolic curve for the x direction. Because the direction of the systematic movement changes with time (the trajectory is curved, i.e., v_y is not zero), the MSD-Δt plot for the y direction is also a parabola (Fig. 4 C). Fitting the curves using Eq. 8, the following values were obtained: $v_x = 22$ nm/s, $v_y = 6$ nm/s, and $D = 3.0 \times 10^{-12}$ cm^2/s (Fig. 4 C).

4. *Restricted diffusion mode*, in which a protein molecule undergoes Brownian diffusion within a limited area and cannot move out of the area during the observation period ($0 \le x \le L_x, 0 \le y \le L_y$). This mode is equivalent to free Brownian diffusion within an infinitely high square well potential. Intuitively, this mode can occur when a membrane protein is trapped within a membrane domain that is formed by the cytoskeleton/membrane skeleton (membrane skeleton fence model) or when a membrane protein is tethered to a loose cytoskeleton (without any restoring potential) that can be extended up to a length of $\sim(L_x^2 + L_y^2)^{1/2}$. (By "loose cytoskeleton" we mean flexible parts of the cytoskeleton, such as an end portion of a thin actin fiber that is not involved in actin bundles or actin meshwork.)

The MSD-Δt plot (Fig. 4, A-c and D) can be expressed as

$$\langle x^2 \rangle(t) = \frac{L_x^2}{6} - \frac{16L_x^2}{\pi^4} \sum_{n=1 \, (odd)}^{\infty} \frac{1}{n^4} \exp\left\{ -\frac{1}{2}\left(\frac{n\pi\sigma_x}{L_x}\right)^2 t \right\} \qquad (11a)$$

$$\langle y^2 \rangle(t) = \frac{L_y^2}{6} - \frac{16L_y^2}{\pi^4} \sum_{n=1 \, (odd)}^{\infty} \frac{1}{n^4} \exp\left\{ -\frac{1}{2}\left(\frac{n\pi\sigma_y}{L_y}\right)^2 t \right\} \qquad (11b)$$

$$\sigma_x^2 = 2D_x, \qquad \sigma_y^2 = 2D_y, \qquad 4D = 2D_x + 2D_y \qquad (12)$$

$$L_r^2 = L_x^2 + L_y^2. \qquad (13)$$

See the Appendix for the derivation of Eqs. 11–12 (for the general case of nonzero v and L). The slope of the curve at time 0 is again $2D_x$ and $2D_y$, and the curve asymptotically approaches $L_x^2/6$ and $L_y^2/6$ in the x and y directions, respectively.

Thus, it would be possible to obtain the diffusion coefficients, the transport velocity, and the constrained area by fitting the above equations to the plot of MSD versus Δt. Fitting was carried out by least-squares analysis using the Gauss-Newton procedure.

Fig. 3 D shows a typical trajectory of a particle undergoing Brownian diffusion, but confined within a limited area. The MSD-Δt curve was fitted using Eq. 11, with $L_x = 88$ nm, $L_y = 128$ nm, and $D = 1.35 \times 10^{-10}$ cm^2/s (Fig. 4 D).

One could not differentiate between the following two models based on the trajectories of the restricted diffusion mode: (a) confinement of a membrane protein within a compartment formed by the cytoskeleton/membrane skeleton (membrane skeleton fence model) due to the lack of space for the cytoplasmic domain of the membrane protein to pass between the membrane and the membrane-skeletal network, and (b) tethering of a membrane protein to a flexible part of the cytoskeleton that can be extended to a certain length with weak forces. For convenience and brevity, we present the following data by assuming the first model, which we believe is more likely. See Discussion for details. In either case, the "confinement model" can be readily converted to the "tethering model."

5. *Obstacle-impeded diffusion mode*, in which free diffusion of a membrane protein is impeded by the presence of obstacles to diffusion such as protein aggregates or protein-rich domain in the membrane. Percolation theory indicates that long-range diffusion will cease altogether if the obstacles are immobile and cover more than a threshold fraction of the surface. For immobile obstacles below the critical threshold and for mobile obstacles at any fractional coverage of the membrane surface, the rate of long-range diffusion is reduced but is still greater than zero (Saxton, 1982, 1987, 1989a, 1990, 1993; Abney et al., 1989). In this case, the MSD-Δt plot can be expressed as (excluding $\Delta t \approx 0$; van Beijeren and Kutner, 1985)

$$\text{MSD}(\Delta t) = 4D\Delta t + A + B \ln C\Delta t \qquad (14)$$

for a quadratic lattice with isotropic jump rates (A, B, C, and D are constants). Due to the somewhat similar behavior of Eqs. 11 and 14, it might be difficult to differentiate between restricted and obstacle-impeded diffusion modes by simply using the MSD-Δt plots. In the present analysis, the percolation effect is likely to appear as smaller D and/or the presence of domains. However, long-term observations ($\sim$6 min) of Tf-R and α_2-macroglobulin receptor indicated that long-range diffusion of these receptor molecules takes place by the movements from one confined domain to adjacent domains (Sako and Kusumi, unpublished observation). This result suggests that confined diffusion observed during a shorter period is not due to the percolation effect. Due to these reasons, we will not explicitly consider the percolation effect in the following part of this paper.

The rate of long-range diffusion may be described by the percolation theory (Saxton 1989a,b, 1990), with the membrane skeleton network serving as a percolation barrier. We

will return to this point when we discuss the movements of EGF-R and Tf-R.

It should be noted that the mode classification is carried out statistically and that the resolution of classification is not clean. However, in the present report, we classify the particles' trajectories into the simple diffusion mode if we cannot exclude the possibility of simple diffusion at a probability better than 97.5% and intend to show the presence of a great fraction of non-Brownian diffusion unequivocally.

Determining the microscopic diffusion coefficient

The diffusion coefficients determined by FPR are influenced by the diffusion processes over micrometer ranges. In particular, these FPR diffusion coefficients are strongly affected by membrane structures, such as the membrane skeleton fence. Although this is a useful feature of FPR diffusion coefficients, the negative aspect of this feature is that one cannot differentiate between the viscosity and structural properties of the membrane using the FPR diffusion coefficient.

The diffusion coefficients determined by SPT can provide the diffusion rate within a submicrometer domain, which only reflects the viscosity properties within a membrane compartment. Therefore, we refer to the SPT diffusion coefficient as the *microscopic* diffusion coefficient. D of each particle is proportional to the differential coefficient of the MSD-Δt plot at time 0.

In this investigation, D was determined by fitting the MSDs at $2\delta t$, $3\delta t$, and $4\delta t$ using a straight line. We refer to the values of D determined by this method as D_{2-4}. Since the behavior of the plot between time 0 and $2\delta t$ is complex, we avoided using this part of the plot. When the time interval used to estimate D was longer than $4\delta t$, in the case of confined diffusion, the effect of the domain boundary on D was apparent. Therefore, we used the time interval between $2\delta t$ and $4\delta t$. In principle, D can be directly estimated by fitting the MSD-Δt plot using Eqs. 5-12. However, the fit near 0 was often poor because the least-squares fit is greatly influenced by points with large Δt. Therefore, when D is determined from the fitting near $\Delta t = 0$, it is believed to be more accurate. D_{2-4} is larger than the values of D determined using Eqs. 5-12 by a factor of 1.2 on average in the case of restricted diffusion, which shows the greatest deviation.

D_{2-4} is convenient because it can be determined independently of the motional modes. This point is important when we classify the particle trajectories into four types of motion. (In theory, the microscopic diffusion coefficient is proportional to the differential coefficient at time 0 in the MSD-Δt plot. Therefore, it does not depend on the motional modes.) When the directed motion is rapid, as is evident during a time period of a few video frames, this analysis cannot be used. However, such fast directed motion was not observed during this study.

The histogram displayed in Fig. 5 shows the number of particles with D_{2-4} in each range. D_{2-4} varies between 2.2 $\times$
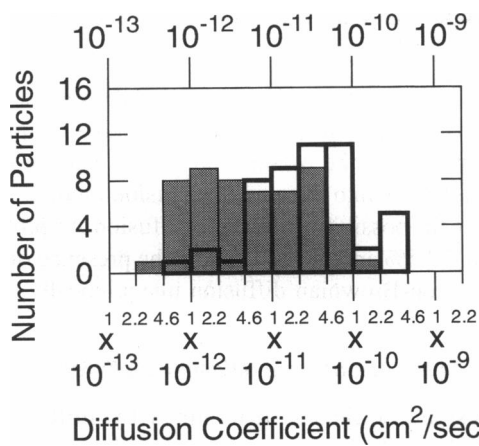
FIGURE 5   A histogram showing the number of particles versus microscopic diffusion coefficient (D_{2-4}) for E-cadherin in the high-calcium (unshaded, thick lines) and in the low-calcium (shaded) mediums.

10^{-13} and 1.0×10^{-9} cm²/s. The diffusion coefficient distribution differs between cells in high- and low-calcium media. The larger number of particles with small values of D_{2-4} in low-calcium cells (Fig. 5) correlates well with the fact that many E-cadherin molecules exhibited the directed diffusion mode in the low-calcium medium, as will be discussed later. (The directed diffusion observed in this work is thought to occur due to binding of the receptors to cytoskeleton undergoing unidirectional motion (Sheetz et al., 1989).)

Determining the motional modes for each trajectory

As mentioned above, four motional modes of membrane proteins are considered here. However, classifying each trajectory during a certain time period into one of these modes is not an obvious matter because of (a) the statistical nature of the problem and (b) interconversion of the motional modes of a particle. For example, the trajectory of a particle that apparently shows directed diffusion (transport) mode may simply be a statistical variation of simple diffusion. Some molecules appear to change the motional modes during observation, or, in the case of the restricted diffusion mode, some appear to move from one domain to the adjacent domain, further complicating statistical analysis.

The MSD-Δt plot shows positive and negative deviations from a straight line with a slope of $4D$ (in the case of two-dimensional diffusion) for directed diffusion and restricted diffusion, respectively (Fig. 4 A). Larger deviations indicate larger probabilities of non-Brownian diffusion. A parameter for the relative deviation, RD(N, n), is defined as

$$RD(N, n) = \frac{MSD(N, n)}{4D_{2-4}n\delta t} \tag{15}$$

where MSD(N, n) represents MSD determined at a time interval $n\delta t$ from a sequence of N video frames. $4D_{2-4}n\delta t$ is the expected average value of MSD for particles undergoing simple diffusion with a diffusion coefficient of D_{2-4} in two-

dimensional space. In the case of simple diffusion, the average RD(N, n) should be 1.

By simulating the movements of particles undergoing simple Brownian diffusion using a computer, we have examined whether this deviation RD(N, n) in the MSD-Δt plot can be used to classify types of motion. In the following discussion, we consider only modes 2, 3, and 4, that is, simple diffusion, directed diffusion, and restricted diffusion modes. The stationary mode is a special case of modes 2 and 4 in which D_{2-4} is smaller than 4.6×10^{-12} cm²/s, and will be considered later.

As discussed by Qian et al. (1991), the statistical variations of MSDs determined from trajectories of single particles (Eqs. 2–4) are different (running average over a single trajectory) from those determined by an ensemble average of a collection of particles. Since the exact functional form of the statistical distribution of MSDs determined from a single particle trajectory is not known, we estimated RD(N, n) by carrying out a computer simulation of movements of particles undergoing simple Brownian diffusion. In the simulation, the step size was kept constant and only the direction of jump for each step was varied randomly. Trajectories for $N = 1000, 500, 300,$ and 200 steps were generated for more than 500 particles; MSD-Δt plots were produced for $n = 90, 150, 300, 360,$ and 720 ($n < N$) steps for each particle (Eqs. 1–4); and then RD(N, n) was determined for each trajectory.

RD(N, n) was used to classify trajectories. Histograms of the number of simulated particles versus RD(N, n) for various N and n values are shown in Fig. 6 (S: top row). From the simulation of Brownian particles, RD(N, n) values that give 2.5% of the particles from both ends of the distribution, referred to as $RD_{min}(N, n)$ and $RD_{max}(N, n)$, were determined and are shown by vertical broken lines. When the trajectory of an experimental particle showed an RD(N, n) value larger than $RD_{max}(N, n)$ or smaller than $RD_{min}(N, n)$, it was classified as having directed or restricted diffusion modes, respectively.

The distribution of RD(N, n) for simulated Brownian particles (Fig. 6, top row) becomes broader as N decreases from 1000 to 300 or n increases from 90 to 720, as expected from Eq. 2 (the variation of MSD(N, n) obtained from single trajectories increases with an increase in n for a fixed N and with a decrease in N for a fixed n). The dependencies of $RD_{min}(N, n)$ and $RD_{max}(N, n)$ on N and n obtained from simulated trajectories are shown in Fig. 7. In the left figure, n is fixed at 90 and $RD_{max}(N, 90)$ and $RD_{min}(N, 90)$ are shown, while in the right figure N is fixed at 1000 and $RD_{max}(1000, n)$ and $RD_{min}(1000, n)$ values are shown. For a given set of (N, n), if the RD(N, n) value for an experimental particle is greater than $RD_{max}(N, n)$, between $RD_{max}(N, n)$ and $RD_{min}(N, n)$, or smaller than $RD_{min}(N, n)$, it is classified as having directed, simple Brownian, or restricted diffusion mode, respectively (see Fig. 7).

Similar histograms for experimental particles attached to E-cadherin are shown in Fig. 6. Movements of 50 particles
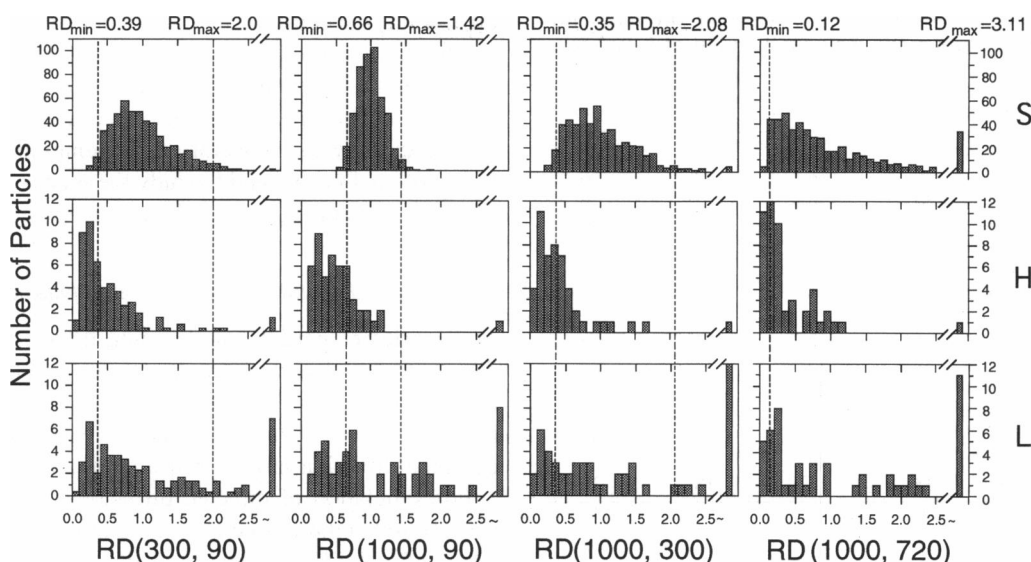
FIGURE 6   Histograms showing the relationships between the number of particles versus $RD(N, n)$. $RD_{min}(N, n)$ and $RD_{max}(N, n)$, as determined from the distribution of $RD(N, n)$ for simulated particles (S: top row), are shown by vertical broken lines. The experimental data for E-cadherin are shown in the middle (H: high-calcium medium) and bottom (L: low-calcium medium) figures. (N, n) pairs shown are (300, 90), (1000, 90), (1000, 300), and (1000, 720).
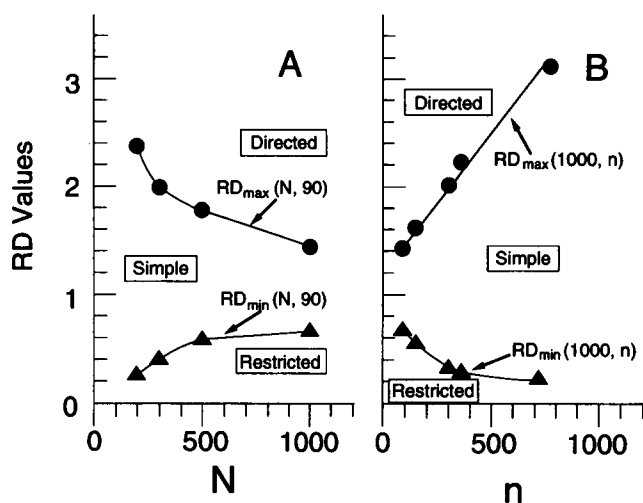

FIGURE 7 $RD_{max}(N, n)$ and $RD_{min}(N, n)$ plotted as a function of N for the fixed value of $n = 90$ (A) and as a function of n for a fixed value of $N = 1000$ (B). The areas bounded by the lines represent simple, directed, and restricted diffusion modes.

in the high-calcium medium (H: middle row) and 54 particles in the low-calcium medium (L: bottom row) were studied. The shape of the histogram for experimental particles is quite different from that for simulated particles. This difference clearly shows the existence of experimental particles undergoing non-Brownian diffusion.

This method has an inherent tendency to underestimate restricted and directed diffusion modes for two reasons:

1. These diffusion modes are determined by deviations from the simple diffusion mode. Since the intrinsic deviation of $RD(N, n)$ from 1 (the variations of MSD) for particles

undergoing Brownian diffusion increases with an increase of n/N (as seen in Fig. 6, top row), non-Brownian diffusion modes become increasingly difficult to discern from simple Brownian diffusion for large n/N. Under these conditions, the distribution of $RD(N, n)$ for simulated Brownian particles becomes broad and, as shown in the right column of Fig. 6 ($N = 1000$, $n = 720$), it becomes very difficult to differentiate other modes from simple diffusion.

2. With the present method of using $RD(N, n)$, only those particles that exhibit restricted and directed diffusion modes for most of N video frames are classified as having these modes. In the case of confined diffusion, if a particle moves from one compartment (domain) to an adjacent compartment during the observation period, it may be classified as exhibiting simple Brownian diffusion. The effect of these problems (interconversion of motional modes and interdomain particle movements) on the mode's classification correlates to the interplay between the time during which a particle exhibits a particular mode (or the residence time of a particle remaining in one domain in the case of the restricted diffusion mode), $N\delta t$, and $n\delta t$. The tendency to overestimate the simple diffusion mode due to interconversion increases as N and n increase.

Since both of these effects are related to N and n, mode classification was performed by varying N and n, as shown in Table 2 (stationary mode; $D_{2-4} < 4.6 \times 10^{-12}$ cm^2/s in the simple or restricted diffusion mode, as discussed in the next subsection). The general tendency is that the percentages of particles classified as exhibiting the restricted and directed diffusion modes decrease and those exhibiting the simple diffusion mode increase with a decrease in N and an increase in n. This result suggests that statistical

TABLE 2 The fraction for each diffusion mode of E-cadherin in high- and low-calcium mediums as a function of N and n

[Ca^{2+}]	N	n	Simple (%)	Restricted (%)	Directed (%)	Stationary (%)
High	1000	90	28	64	2	6
	1000	150	26	66	2	6
	1000	300	36	56	2	6
	1000	720	62	30	2	6
	500	90	36	55	3	6
	300	90	37	51	4	8
	200	90	56	33	3	8
Low	1000	90	11	30	37	22
	1000	150	11	31	31	26
	1000	300	26	24	28	22
	1000	720	37	13	19	31
	500	90	19	26	26	30
	300	90	25	19	19	37
	200	90	33	13	18	36

variations in MSD(N, n), and therefore in RD(N, n), rather than the frequency of mode interconversion limits the accuracy of mode classification in the case of E-cadherin in the F7p plasma membrane.

In the present paper, we used $N = 1000$ and $n = 90$ for the mode classification because the distribution of RD(N, n) at these values is sharp. In addition, the error in the estimate of experimental RD(N, n) using Eq. 17 decreases as n/N decreases. Finally, mode interconversion is not serious in the 30-s time range, as seen by comparing the data for (N, n) = (1000, 90) with those for (500, 90) (Table 2).

In the case of restricted diffusion, the interplay between D, the time interval (n), and the size of the confined domain ($L_x L_y$) should be noted. Due to the relationship $\langle r^2 \rangle = 4Dn\delta t$, as the size of the compartment increases, the existence of the compartment becomes increasingly more difficult to detect for constant D and n. Since a particle with $D = 10^{-9}$ cm^2/s, which is close to the maximum D value observed in this work, will cover an area of 1 μm^2 over 3 s ($n = 90$ steps), the present method can only detect membrane domains comparable to or smaller than 1 μm^2. Therefore, the percentages of particles in the restricted and simple diffusion modes are n-dependent. Observations for longer time intervals should allow the detection of larger membrane domains. However, as n increases, N should be increased by the same percentage as the increase in n to achieve similar statistical accuracy. To achieve $n = 900$, which would enable observation of a domain up to 10 μm^2, N should be 9000, which makes experiment difficult and makes the time needed to calculate the positions of gold particles inhibitively long ($\sim$7 h for each trajectory). Therefore, to observe domains larger than 1 μm^2, other methods such as dragging of the colloidal gold-protein complex in the membrane by a laser optical trap may be more suitable (Edidin et al., 1991; Sako and Kusumi, in preparation).

Some particles showed the restricted diffusion mode in one direction (e.g., the x direction) and the simple diffusion mode in the other direction. Even if a particle is confined in only one direction, it can be classified as exhibiting restricted

diffusion if the confined length is small. This is because the classification was made based on two-dimensional diffusion.

Despite the reservations and limitations discussed above, we think that this method provides a convenient and practical way to classify the trajectories of membrane proteins into four motional modes and to study the mechanism that regulates the movements of membrane proteins.

Accuracy and limitations of the mode classification

Trajectories of particles undergoing directed and confined diffusion were generated in a computer, and the accuracy of the classification method above was evaluated. In addition, limiting v and L values for classification into directed and confined diffusion modes, respectively, were estimated.

For simulation of directed diffusion, a velocity v is superimposed in the x direction on random diffusion. To simulate confined diffusion, elastic walls are placed at $-L/2$ and $L/2$ in both the x and y directions. Eight thousand trajectories of $N = 1000$ steps were generated for each L^2/D or v^2/D value, and a histogram of RD(1000, 90) was obtained for each L^2/D or v^2/D value (Fig. 8, A and B, respectively). From the histograms for $L = \infty$ (Fig. 8 A) and $v = 0$ (Fig. 8 B), which correspond to simple Brownian cases, RD$_{min}$ and RD$_{max}$ were determined (2.5 percentile values from both ends of the distribution). As L becomes greater or v smaller, the histograms show more areas overlapped with those for purely Brownian diffusion, and more particles are classified as simple diffusion. L^2/D and v^2/D values that give 50% and 95% probability of being classified into directed and confined diffusion modes are $L^2/D = 29$ and 15 ($L = 540$ nm
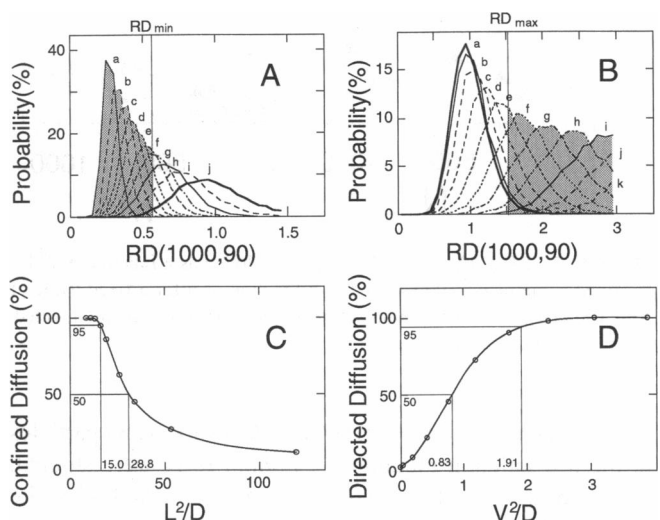

FIGURE 8 (A and B) Histograms of RD(1000, 90) for the cases of confined (A) and directed (B) diffusion. The ordinates are the percentages of the number of occurrences. In A, L^2/D values for different histograms are 8.50 (a), 10.8 (b), 13.3 (c), 16.1 (d), 19.1 (e), 26.0 (f), 34.0 (g), 53.2 (h), 119.6 (i), and ∞ (j). In (B), v^2/D values are varied from 0 (a), 0.0478 (b), 0.191 (c), 0.431 (d), 0.765 (e), 1.196 (f), 1.722 (g), 2.344 (h), 3.061 (i), 3.875 (j), and 4.783 (k). The curves (histograms) j in (A) and a in (B) are based on the (basically) same data but in different intervals in abscissas. (C and D) probabilities of classifying given trajectories into confined (C) and directed (D) diffusion modes for various L^2/D (C) and v^2/D values (D).

and 390 nm in the case of $D = 10^{-10}$ cm^2/s) and $v^2/D = 0.83$ and 1.91 ($v = 91$ nm/s and 140 nm/s in the case of $D = 10^{-10}$ cm^2/s). L^2/D values for trajectories B, D, and F in Fig. 3 are 90.9, 11.3, and 50.2, respectively (L could not be determined for B and E). The v^2/D value for C is 3.14, while those for B, E, F are $\sim$0 (v could not be determined for D).

The overlaps of the histograms indicate that clear classification of motional modes is impossible, as described by Saxton (1993). The method used in this work, however, unequivocally determines (with 2.5% uncertainty) non-Brownian diffusion (thus overestimating the simple diffusion). In this sense, readers are reminded to be careful about the semantics of the words "simple," "directed," and "restricted diffusion." From the viewpoint of biological significance, detection of non-Brownian diffusion is useful. Comparison of RD histograms for simulated (Brownian) and experimental particles shown in Fig. 6 also clearly indicates that the dominant nature of E-cadherin movements is non-Brownian. The probabilities of being classified into directed and confined diffusion modes for given L^2/D and v^2/D values, respectively, are shown in Fig. 8, C and D. Further development of analysis methods is required to detect the restricted and directed diffusion modes more sensitively. Saxton (1993) has proposed a different approach.

Determination of the stationary mode

As described above, all particles attached to E-cadherin show D_{2-4} larger than 2.2×10^{-13} cm^2/s, that is, these particles are not completely stationary. However, FPR measurements of E-cadherin showed that approximately one-third of the cadherin molecules are immobile. Since the bleached and observed area is large ($\sim$0.9 μm in diameter) compared with the nanometer-level resolution of the SPT method, the immobile component observed by FPR would include both stationary molecules (which have very small D) and some of those confined in a membrane subdomain within the observed area.

As an approach to determining the stationary mode by SPT, D_{2-4} for particles showing the directed diffusion mode was examined. Most receptor molecules with this mode may be tightly associated with cytoskeletal elements that are moving unidirectionally. Therefore, the movements of the receptor molecules reflect small random motion superimposed on the unidirectional movements. These D values may provide a guideline for D for stationary molecules that are associated with the rigid part of the stationary cytoskeleton. A histogram of the number of particles versus D_{2-4} in the directed diffusion mode is presented in Fig. 8 (average $v = 19 \pm 3$ nm/s). Since this mode appears only in the low-calcium medium, only the histogram for the low-calcium condition is shown (20 of 54 and one of 50 particles were determined to exhibit this mode in low- and high-calcium mediums, respectively). The distribution of D_{2-4} is complex but shows the presence of a broad peak at 2.2×10^{-13} to 4.6×10^{-12} cm^2/s, which represents 70% of particles that exhibit the directed diffusion mode. These E-cadherin molecules are

probably attached to cytoskeleton undergoing unidirectional motion, since the lipid flow model cannot explain such small D values. It has been suggested that E-cadherin is attached to actin filaments (Hirano et al., 1987; Kemler and Ozawa, 1989; Kusumi et al., 1990). Involvement of the cytoskeleton in this mode was further confirmed by incubating the cells in the medium containing cytochalasin D or vinblastin, which are known to disrupt actin filaments and microtubules, respectively. Treatment with these chemicals completely abolished the directed diffusion mode (data not shown).

The small random motion observed for $\sim$70% of E-cadherin molecules exhibiting the directed diffusion mode may be due to structural fluctuation of the cytoskeleton and the plasma membrane. Since the major cause of the stationary mode is likely to be association with the cytoskeleton, the D values for the stationary mode should be close to those for the directed diffusion mode (e.g., D for E-cadherin bound to stationary cytoskeleton). On the basis of the histogram in Fig. 9, we classify particles with $D_{2-4} \leq 4.6 \times 10^{-12}$ cm^2/s as having the stationary mode. This number is somewhat arbitrary. However, changing it to 1.0×10^{-11} cm^2/s does not affect the conclusion of this paper. In addition, this value is close to the limitation of D measurement using the FPR technique ($\sim$3 $\times 10^{-12}$ cm^2/s) (Axelrod et al., 1976).

To summarize the criteria for the stationary mode, if a particle is judged to exhibit simple or restricted diffusion mode based on RD(1000, 90) from the MSD-Δt plot (Figs. 6 and 7), and if it has D_{2-4} less than 4.6×10^{-12} cm^2/s, it is classified as having the stationary mode. If a particle is determined to have directed diffusion mode, the value of D_{2-4} does not affect the classification (it is still classified as having the directed diffusion mode).

Characteristics of receptor movements

Motional modes for E-cadherin, EGF-R, and Tf-R in high- and low-calcium mediums

E-cadherin (M_r 124,000) and EGF-R (M_r 170,000) have single transmembrane domains, while Tf-R (M_r 180,000) has two such domains. Tf-R is a homodimer consisting of two identical polypeptides. The sizes of the cytoplasmic domains
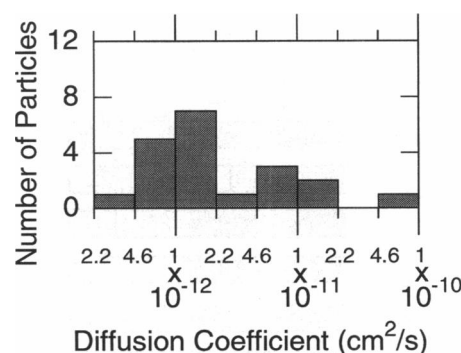

FIGURE 9   Histogram of the number of particles versus D_{2-4} for E-cadherin molecules classified into the directed diffusion mode in the low-calcium medium.

are 152, 542, and 61 $\times$ 2 amino acids, for E-cadherin (Nagafuchi et al., 1987), EGF-R, and Tf-R (Goldstein et al., 1985), respectively. E-cadherin molecules are thought to be associated with some or all types of catenins (α-, β-, and γ-catenins, the M_r of which are 102,000, 88,000–94,000, and 80,000, respectively; Ozawa et al., 1989, 1990; McCrea and Gumbiner, 1991) in its cytoplasmic domain. Therefore the cytoplasmic domain of the cadherin-catenin complex is large. Some of the cadherin-catenin complexes are likely to be associated with the actin filaments (Hirano et al., 1987; Kemler and Ozawa, 1989). EGF-R has been shown to bind to actin via a domain containing amino acid residues 984–996 (den Hartigh et al., 1992).

Motional modes for E-cadherin molecules are shown in Fig. 10. The motional modes are different between high- and low-calcium mediums. The primary difference is the decrease in the percentage of the restricted and the simple diffusion modes, and the enhancement of the directed diffusion and stationary modes in the low-calcium medium. The trajectories of the particles that showed directed diffusion with $D < 3 \times 10^{-12}$ cm^2/s (70% of the directed diffusion case) are represented by the one shown in Fig. 3 C. (Other trajectories in this mode with $D > 3 \times 10^{-12}$ cm^2/s look like larger diffusional motion in a narrow strip.) If we assume that the directed diffusion and stationary modes are due to binding of E-cadherin to the cytoskeleton, $\sim$60% of cadherin molecules on the dorsal cell surface are bound to the cytoskeleton in the low-calcium medium. Such an increase in the cytoskeleton-bound fractions was not observed for EGF-R and Tf-R in the low-calcium medium (Fig. 10), indicating that such calcium-induced changes are specific to E-cadherin and not due to overall structural changes of the plasma membrane. Association with the cytoskeleton may be related to the movement and assembly of E-cadherin to the cell-cell contact regions during the initial stages after the calcium switch.

Relatively minor differences in the motional modes between the two calcium conditions were observed for Tf-R. The molar ratio of the receptors showing the restricted versus the simple diffusion modes is 2.7 and 1 in high- and low-calcium mediums, respectively. The sum of the directed dif-

fusion and the stationary modes, which presumably reflects the number of particles bound to the cytoskeleton, is about the same ($\sim$12%) in both mediums. In the case of EGF-R, the percentages of molecules showing the simple and restricted diffusion modes are about the same for the two mediums, while the percentages of molecules showing the stationary and the directed diffusion modes in the high-calcium medium were smaller and greater than the respective percentages in the low-calcium medium (both of these modes presumably involve binding to the cytoskeleton, and their sums are unchanged).

The average D_{2-4} vaules for E-cadherin, EGF-R, and Tf-R in simple and restricted diffusion modes are summarized in Table 3. Histograms of the number of particles versus D_{2-4} are shown in Fig. 11. The diffusion coefficients vary greatly from particle to particle, with a range of 4.6 $\times$ 10^{-12} to 1 $\times$ 10^{-9} cm^2/s. Vaules of D_{2-4} for EGF-R are generally greater than those for other receptors (Table 3). Little difference in D_{2-4} was observed between the simple and restricted diffusion modes for the same protein species. The diffusion coefficients for EGF-R and Tf-R are independent of the Ca^{2+} concentrations in the medium.

We think that the restricted diffusion mode occurs due to confinement of receptor molecules within compartments (for finite duration). This is also supported by the following unpublished observations (to be published elsewhere): (*a*) Long-term observation ($\sim$6 min) of receptor movements showed repeated sequences of intracompartment diffusion and intercompartmental movements from one domain to adjacent domains. The average residence time within a compartment (domain) is $\sim$25 s. (*b*) Deletion of the cytoplasmic domain of E-cadherin greatly increases the size of the confined area or eliminated confinement, suggesting that the cytoplasmic domains are involved in the restricted diffusion mode. (In general, the extracellular surface of the membrane is more crowded than the intracellular surface (Sheetz, 1993).) (*c*) Forced movements of the receptor-gold particle complexes by a laser tweezer indicated the presence of compartmental boundaries (barriers).

If the meshwork of membrane-associated cytoskeleton (membrane skeleton) forms an obstacle to diffusion with breaks in time and space (Tsuji, et al., 1988; Saxton, 1989b), obstacle-impeded percolation diffusion should be a useful model for long-range diffusion over many cytoskeletal meshes.

The size of the membrane domain

For the restricted diffusion mode, the area of confinement, defined as $L_x \times L_y$, and the diagonal length of the area, defined as $(L_x^2 + L_y^2)^{1/2}$, were evaluated using Eq. 11. The distributions of the area size are shown in Fig. 12. The average size and the diagonal length of the confinement area are summarized in Table 4, which indicates that the domain is 300–600 nm in diagonal length and 0.04–0.24 μm^2 in area. The confined domain tends to be smaller in cells cultured in

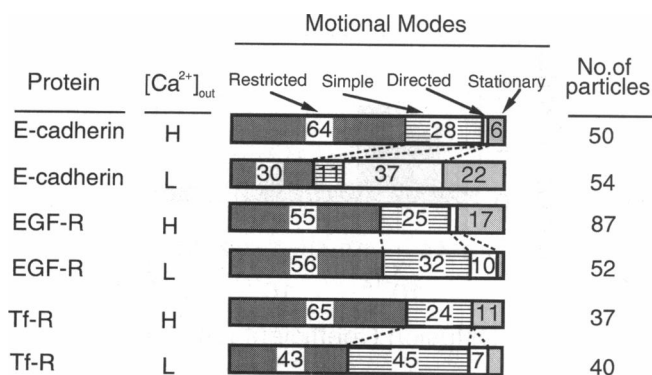| Protein	[Ca^{2+}]$_{out}$	Restricted	Simple	Directed	Stationary	No. of particles
			Motional Modes			
E-cadherin	H	64		28	6	50
E-cadherin	L	30	11	37	22	54
EGF-R	H	55		25	17	87
EGF-R	L	56		32	10	52
Tf-R	H	65		24	11	37
Tf-R	L	43		45	7	40

FIGURE 10   Fractions of E-cadherin, EGF-R, and Tf-R molecules exhibiting various diffusion modes in high- and low-calcium media.

TABLE 3 D_{2-4} (±SD, × 10⁻¹¹ cm²/s) of E-cadherin, EGF-R, and Tf-R in the plasma membrane of mouse keratinocytes in high- and low-calcium mediums measured at 36.5°C

Receptors	High-calcium medium		Low-calcium medium	
	Restricted diffusion	Simple diffusion	Restricted diffusion	Simple diffusion
E-Cadherin	6.5 ± 7.9 (64)	5.5 ± 6.0 (28)	3.3 ± 2.9 (30)	3.2 ± 2.7 (11)
EGF-R	11.2 ± 15.0 (55)	14.7 ± 12.7 (25)	10.4 ± 7.8 (56)	20.5 ± 22.1 (32)
Tf-R	7.8 ± 8.1 (65)	4.4 ± 3.5 (24)	5.6 ± 4.8 (43)	4.4 ± 4.8 (45)

The large SDs indicate, in addition to the experimental error, the real variation in D_{2-4} for individual particles. Numbers of particles studied: 50 and 54 for E-cadherin, 87 and 52 for EGF-R, and 37 and 40 for Tf-R in the high- and low-calcium mediums, respectively. Numbers in parentheses, percentage of particles showing the mode.
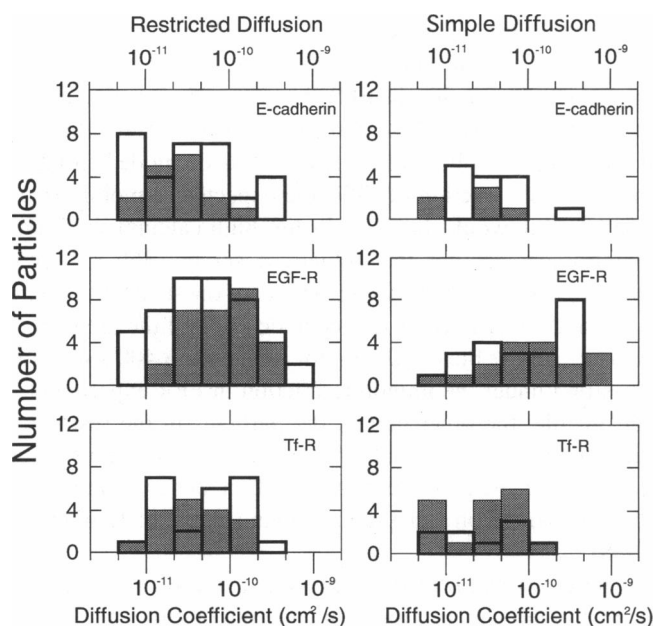

FIGURE 11 Histograms showing the number of particles versus D_{2-4} for particles exhibiting the restricted diffusion mode (*left*) and the simple diffusion mode (*right*) in the high-calcium (*unshaded, thick lines*) and in the low-calcium (*shaded*) mediums. Data for E-cadherin (*top*), EGF-R (*middle*), and Tf-R (*bottom*) are shown.

FIGURE 12 Histograms showing the number of particles versus the confined area (L_xL_y) for particles exhibiting the restricted diffusion mode. Data for E-cadherin (*top*), EGF-R (*middle*), and Tf-R (*bottom*) in the high-calcium (*unshaded, thick lines*) and in the low-calcium (*shaded*) mediums are shown.

the low-calcium medium. The domain size "felt" by the receptors tends to be smaller for E-cadherin. This may be due to the larger size of the complex of three catenins and the cytoplasmic domain of E-cadherin (M_r ~290,000) than the cytoplasmic domains of other receptors.

One of the aims of the present work is to obtain information regarding the structure of the membrane domain as it is "felt" by the receptor molecules and to test the "membrane skeleton fence model" (Tsuji et al., 1988; see Introduction). The membrane skeleton fence model proposes that free diffusion of membrane proteins is interrupted due to steric hindrance from the membrane-associated cytoskeleton meshwork; the space between the membrane and the cytoskeleton is too small for the cytoplasmic portion of the membrane protein to pass, thus limiting the free diffusion of receptors into small domains bounded by the membrane skeletal meshwork. Thus, with regard to the diffusion of membrane proteins, the membrane is compartmentalized into many small domains. The present results are consistent
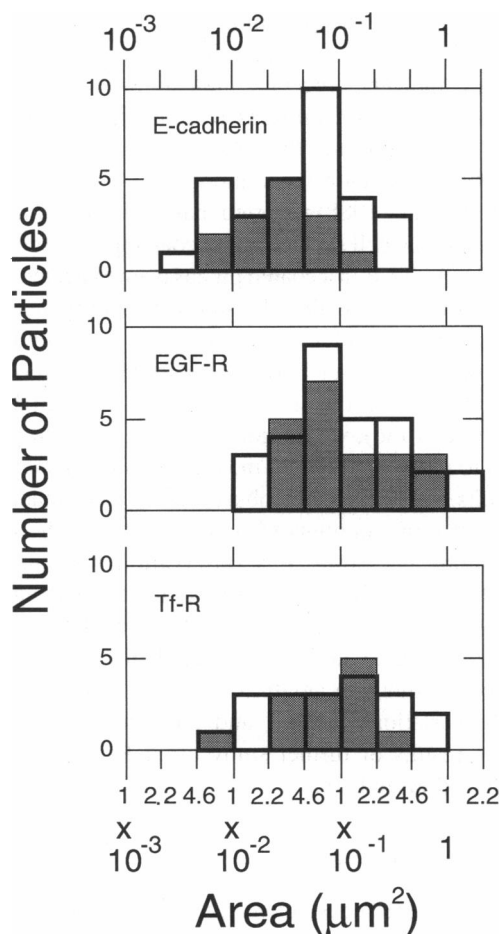
with this model and indicate that the domain has a diagonal length of 300–600 nm.

The model also proposes that the membrane proteins can escape from one domain to adjacent domains due to the dynamic properties of the membrane skeleton. The distance between the membrane and the skeleton may fluctuate over time, thus giving the membrane proteins an opportunity to pass the barrier of the mesh. The membrane skeleton may dissociate from the membrane, and the membrane-skeleton

TABLE 4 Sizes of the membrane domains detected by observation of receptor movements

Receptors	Area of confinement (μm^2)		Diagonal length of the area (nm)	
	High-calcium	Low-calcium	High-calcium	Low-calcium
E-cadherin	0.076 ± 0.075	0.042 ± 0.045	360 ± 190	270 ± 130
EGF-R	0.24 ± 0.38	0.19 ± 0.21	620 ± 450	580 ± 340
Tf-R	0.16 ± 0.18	0.10 ± 0.070	570 ± 440	480 ± 250

network may form and break continuously due to dissociation-association equilibrium of the cytoskeleton. If this model is correct, the size of the compartment "felt" by receptor molecules may depend on the size of the cytoplasmic domain of the receptor molecules. The membrane domain size for E-cadherin, which has larger cytoplasmic domains than the other receptor molecules examined due to binding of associated proteins (catenins), is smaller than those of other receptors; this observation again agrees with the membrane skeleton fence model.

Iacopetta et al. (1988) reported that ~15% of human Tf-R molecules on the cell surface are in coated pits in transfected mouse L-cells. Tf-R in a coated pit has been expected to show little mobility. Meanwhile, the stationary component in the present study is smaller (5–11%). Since many endosomes containing Tf-gold and EGF-gold particles were observed inside cells (which agrees well with the result of De Brabander et al., 1986), we do not think that the gold particles attached to receptors prevent the receptors from entering the coated pits. (Note that our observations were made in the presence of large amounts of gold particles in the incubating medium. Therefore, this observation was made at a steady state of binding of gold particles to Tf-R and internalization of gold-labeled Tf-R). We speculate that some receptors in coated lattices or coated pits are still somewhat mobile, showing small D and/or L. This may explain the large variations in D_{2-4} and the size of the confined area. The results of further study of Tf-R movements will be published elsewhere.

Comparison with FPR results

A remarkable difference between SPT and FPR observations of E-cadherin movements is that the fraction of the stationary component in SPT differs from the immobile fraction in FPR in the high-calcium medium (Table 1). In FPR measurements, 36% of E-cadherin molecules on the dorsal/apical cell surface (i.e., excluding those at the cell-cell contact sites) were classified into the immobile fraction in the high-calcium medium. In contrast, only 6% of E-cadherin-bound particles are classified as being in the stationary mode in SPT under identical conditions.

E-cadherin molecules that are classified into the stationary mode in SPT ($D < 4.6 \times 10^{-12}$ cm^2/s) are likely to belong to the immobile fraction in FPR. Typical experimental conditions for FPR in the present investigation were a bleached area of 0.63 μm^2 and an observation time of 400 s. Therefore, molecules with diffusion coefficients smaller than 4×10^{-12} cm^2/s would stay within the bleached area during the observation period.

E-cadherin molecules that have been classified into the restricted diffusion mode by SPT may contribute to the immobile fraction in FPR. That is, some proteins that are confined in a membrane subdomain within the bleached area may not escape from the bleached area during the observation period of FPR and would therefore be classified under the immobile fraction in FPR but under the restricted diffusion mode in SPT (Vaz et al., 1989). If we assume that all particles that exhibit the restricted diffusion mode belong to the immobile fraction of FPR, the expected immobile fraction of FPR would be 70% in the high-calcium medium, which is greater than that actually observed (36%). Therefore, it is concluded that approximately one-half of the particles in the restricted diffusion mode (30% of the total number) stay in the bleached area for longer than 400 s and are classified under the immobile fraction in FPR experiments. Meanwhile, the other half of the particles in the restricted diffusion mode occasionally move to adjacent domains, as in the case of band 3, and diffuse out of the observed area (see the next paragraph and Tsuji and Ohnishi, 1986; Tsuji et al., 1988).

These results differ from the conclusion we obtained for band 3 in human erythrocyte membrane (Tsuji et al., 1988). The immobile fractions of band 3, as determined by measurements of both lateral and rotational diffusion, are identical over a wide range of temperature and under various conditions that modify the membrane skeleton of the erythrocyte ghost. This led to the conclusions that the immobile fraction of FPR is due to band 3 molecules bound to the membrane skeleton and that there are no band 3 populations that are captured in the spectrin network during the FPR observation period. It follows then that, in the case of the membrane skeleton in human erythrocytes, either there is an abundance of open gates or the gates open and close frequently; that is, the probability of a gate being open is large (see the Introduction for more information on band 3 motion and Saxton, 1991).

As another method of comparing SPT and FPR, the ensemble-averaged MSD for E-cadherin was calculated by averaging the motion of a collection of trajectories for independent particles (not an average over a single trajectory). When the average was taken, particles in the stationary mode were excluded, since these particles must belong to the immobile fraction in the FPR measurement (note that all trajectories classified into simple, restricted, and directed diffusion modes were included for averaging). Forty-seven and 34 particles were averaged in the high- and low-calcium mediums, respectively. The plots of the ensemble-averaged MSDs versus Δt are shown in Fig. 13. The plots are simple
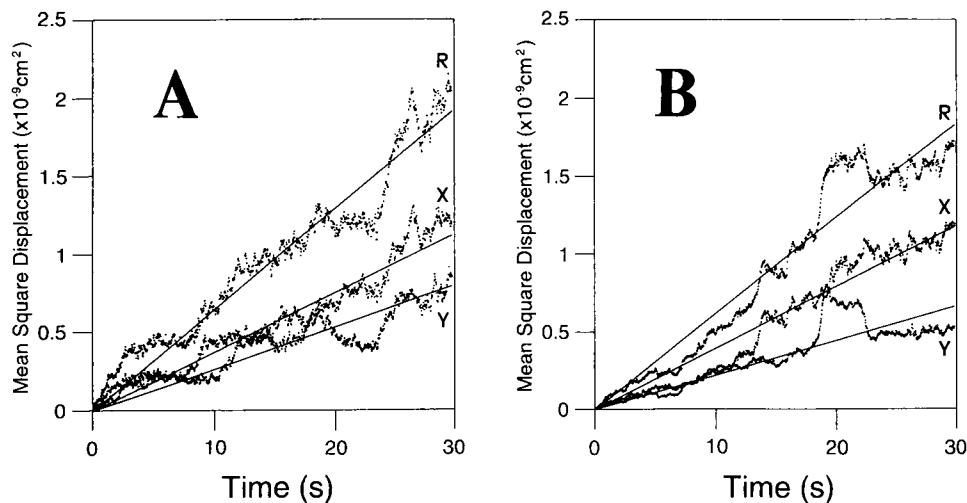
FIGURE 13 Plots for MSD versus Δt obtained by an ensemble-average of a collection of particles attached to E-cadherin in high- (A) and low-calcium (B) media. Particles exhibiting the stationary mode were omitted. By fitting the plot using Eq. 5 (assuming simple diffusion), $D = 1.6$ and 1.4×10^{-11} cm^2/s were obtained for high- and low-calcium conditions, respectively. These values are listed as the macroscopic diffusion coefficients determined by SPT in Table 1. X, Y, and R here indicate diffusion in horizontal and vertical directions in the video frames and in a two-dimensional plane, respectively. Note the difference in the definitions of X and Y between here and other parts of this paper (in which the x direction is the direction of greatest movement).

diffusion-like, and the macroscopic diffusion coefficients estimated from the slopes are 1.6 and 1.4×10^{-11} cm^2/s in high- and low-calcium mediums, respectively. The macroscopic diffusion coefficients determined by FPR are 3.4 and 2.6×10^{-11} cm^2/s in the high- and low-calcium mediums, respectively, indicating a reasonable agreement between the values obtained by the two techniques (Table 1). Since some gold particles in the restricted diffusion mode would not contribute to macroscopic diffusion in this time range (30 s), the macroscopic diffusion coefficients from SPT would be underestimated. Another possible reason for the smaller macroscopic D from SPT may be the multiple binding of E-cadherin to some of the gold particles. A gold particle that is bound to two or three cadherin molecules may have D_{2-4} values similar to that of a gold particle bound to a single cadherin molecule within the domain (Saffman and Delbrück, 1975), but the complex would have less opportunity to move over the membrane skeletal barriers or to pass through the open gate to move to adjacent domains. However, the reasonable agreement of the macroscopic diffusion coefficients determined by the two methods supports the reliability and accuracy of the SPT technique for observing the movements of membrane proteins. Smaller diffusion coefficients for SPT than for FPR were previously reported by Lee et al. (1991) for the movements of a phospholipid analogue, fluorescein-phosphatidylethanolamine, and its complex with gold particles via anti-fluorescein.

Fig. 13 clearly shows that a variety of motional modes observed for individual particles disappeared when the movements of only 47 or 34 particles are averaged (Fig. 13), and deviations from simple Brownian diffusion became difficult to detect. In particular, the directed diffusion mode, which is attributed to as many as 37% of the particles in the low-calcium medium by SPT, is hardly detectable after averaging. The FPR recovery curves also did not show any sign of directed diffusion at the signal-to-noise level obtained in

this work. This result clearly indicates the importance of observing receptor movements at the level of individual molecules (or complexes of a few molecules) for investigation of elementary processes that regulate movements and assembly of these receptor molecules in the plasma membrane.

The average D_{2-4} values determined by SPT were 6.2 and 3.3×10^{-11} cm^2/s, in high- and low-calcium mediums, respectively (Tables 1 and 3). The step size for a particle with these D_{2-4} values between two video frames (33 ms) is $\sim$29 and 21 nm, respectively. In contrast, FPR is sensitive to membrane structures at the micron level. The macroscopic diffusion coefficients for the mobile fraction (64% and 75%) were 3.4 and 2.6×10^{-11} cm^2/s in high- and low-calcium mediums, respectively. The difference between the macroscopic (micron scale by FPR) and microscopic (nanometer scale by SPT) diffusion coefficients is particularly marked in the high-calcium medium. This difference between D_{2-4} and D(FPR) can for the most part be explained by the presence of the restricted diffusion mode in SPT; although diffusion is not significantly restricted at the nanometer level within the confined domain, the movements of a particle at the micron level are slower due to the time needed to pass barriers every 300–600 nm.

On the other hand, the microscopic diffusion coefficients observed here are still small compared with that expected for an integral membrane protein in a lipid bilayer ($\sim 10^{-9}$ cm^2/s). Mechanisms to slow the movements of these receptors must exist, such as the crowding effect due to high concentrations of proteins in the membrane (Saxton, 1982, 1987; Ryan et al., 1988) or binding to loose cytoskeleton (thereby the cytoskeleton acts as an effective load, thus slowing movement) with which the receptor molecules still move by dragging it.

The lateral diffusion of EGF-R and its interaction with the cytoskeletal elements have been studied in mouse 3T3 cells, human A-431 cells, and monkey COS cells that were trans-

fected with a complementary DNA construct of human EGF-R (Hillman and Schlessinger, 1982; Schlessinger et al., 1983; Livneh et al., 1986; Landreth et al., 1985; Wiegant et al., 1986). EGF-R was recently shown to be an actin-binding protein (den Hartigh et al., 1992). Livneh et al. (1986) showed that approximately 40% of EGF-R molecules are immobile in FPR measurements and that the diffusion coefficient for the mobile component is $\sim 1.5 \times 10^{-10}$ cm^2/s. Detergent solubilization extracted only 20–40% of EGF-R molecules from epidermoid carcinoma (A431) cells (Landreth et al., 1985; Wiegant et al., 1986), suggesting that 60–80% of EGF-R molecules are bound to the cytoskeleton. These values differ greatly from the stationary component as determined by SPT (2–17%), although D_{2-4} estimated by SPT is quite similar to D(FPR). Taken together, these results raise the possibility that significant percentages of EGF-R molecules in the restricted diffusion mode are associated with a flexible part of the membrane-skeletal/cytoskeletal system. We have already pointed out that some receptor molecules attached to coated lattices or coated pits may be mobile. In the case of E-cadherin, as shown in Fig. 9, $\sim 30\%$ of particles that are classified as having the directed diffusion mode show D_{2-4} values between $1-10 \times 10^{-11}$ cm^2/s, suggesting that some membrane skeletons or cytoskeletons are flexible and mobile. Since FPR data regarding EGF-R are not available for the present cell type, we refrain from further speculation.

DISCUSSION

One of the most useful ways to study the interactions between the membrane and the cytoskeleton and between membrane proteins is to monitor the movements of membrane proteins. SPT provides information concerning the dynamics of membrane proteins that was not previously available (Sheetz et al., 1989, 1990; Kucik et al., 1989; Mecham et al., 1991; De Brabander et al., 1988, 1991). In the present investigation, we have developed methods to classify the movements of membrane proteins into four categories and to obtain the microscopic diffusion coefficient, the size of the domain, and the transport velocity. A general formula to describe the random diffusion in the presence of reflecting walls and a uniform velocity has been obtained (Appendix).

The movements of three membrane receptors were observed on the dorsal (apical) cell surface of the mouse keratinocytes in culture. Substantial percentages (50–75%) of all of the receptors examined here exhibited the restricted and simple diffusion modes. The average size of the domains that were covered by particles exhibiting the restricted diffusion mode is 300–600 nm in diagonal length and 0.04–0.24 μm^2 in area.

We propose that hindrance of the free diffusion of integral membrane proteins due to the barrier effect of the membrane skeleton is a basic feature of the plasma membrane (membrane skeleton fence structure). In this sense, the plasma membrane is compartmentalized by the net-

work of the membrane skeleton, which has a mesh size of 300–600 nm (see the model presented in Fig. 14). We have shown data to support this proposal only for keratinocytes and the red blood cell. However, we have recently obtained similar data for normal rat kidney fibroblast cells and Chinese hamster ovary cells (unpublished observation).

Similar trajectories would be obtained if the receptor molecules were tethered to the loose part of the cytoskeleton. However, we do not think this is likely. When a receptor-gold complex is dragged back and forth in the plane of the membrane by moving a laser optical trap, the complex often escapes from the trap at the same place regardless of the direction of the movement (unpublished data). These results can be readily explained by the membrane-skeleton fence model but not by the tethering model.

We speculate that the membrane-skeleton fence structure is present over the entire cytoplasmic surface of the plasma membrane, except at special functional domains such as coated pits and cell adhesion structures. In these functional domains, other undercoat structures are present on the cytoplasmic surface. The particles that exhibited the simple diffusion mode may have small D_{2-4} or may be located in larger compartments. In the time scale of observation used in this work (3–30 s), membrane domains larger than 1 μm^2 cannot be observed. The simple diffusion mode was observed probably because some domains were larger than 1 μm^2, and their boundaries could not be detected in the time scale of 3–30 s. We propose that long-range diffusion occurs by the movement of receptors from one compartment to an adjacent compartment.

The membrane-skeleton fence structure agrees with the results of Edidin et al. (1991). They performed experiments in which gold-particle-labeled membrane receptors (major histocompatibility complex class I molecules) were dragged laterally in the membrane with a laser optical trap and found that the "barrier free path length" is 0.6 and 1.7 μm for the transmembrane and glycosylphosphatidylinositol-anchored species, respectively. A similar idea has been proposed by
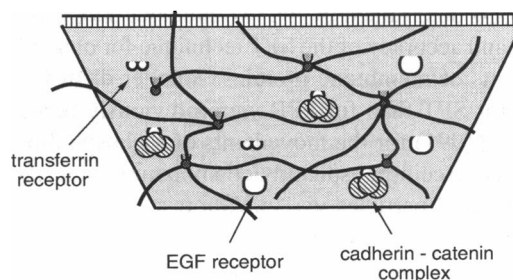

FIGURE 14 A schematic drawing showing the membrane-skeleton mesh, which acts as a fluctuating barrier for the diffusion of membrane proteins (membrane-skeleton fence model). Due to fluctuation in the distance between the membrane and the meshwork and to the connection-disconnection equilibrium of the meshwork, the membrane receptors can move from one compartment to adjacent compartments.

Sheetz et al. (1980) based on experiments using spectrin-defective red blood cells.

Nevertheless, the microscopic diffusion coefficients determined by SPT (Fig. 11) are still smaller than those expected for free Brownian diffusion of proteins in a sea of excess lipids, such as those observed in lipid-rich reconstituted membranes (Peters and Cherry, 1982; Vaz et al., 1984). This may be due to (a) the presence of a high concentration of proteins in the membrane (not near the percolation threshold), (b) the presence of protein clusters in the membrane, (c) binding to the loose part of the cytoskeleton, and/or (d) transient binding to (protein attached to) the cytoskeleton. This problem is yet to be solved.

It is concluded that confined diffusion of integral membrane proteins due to the membrane-skeleton fence structure is a basic feature of the receptor dynamics in the plasma membrane of animal cells and that, for individual protein species, additional specific regulation mechanisms, such as binding to associated proteins (such as catenins for E-cadherin) and binding to the cytoskeleton, may be at work, which are in effect superposed on the barrier effect of the membrane skeleton fence. In studies on receptor aggregation for cellular signaling and formation of special membrane domains, the influence of the membrane-skeleton fence structure must be considered.

CONCLUSIONS

1. SPT has enabled observations of receptor dynamics that were not possible by measuring the average behavior of membrane proteins using FPR (Figs. 10 and 13). Observation of receptor dynamics at the level of single molecules is particularly important for the investigations of elementary processes that regulate the association and assembly of receptors and the formation of special functional domains in the membrane.

2. The movements of receptors in the plasma membrane during a period of 3–30 s can be classified into (a) the stationary mode, (b) the simple diffusion mode, (c) the directed diffusion mode, and (d) the restricted diffusion mode (Fig. 9). Methods for mode classification and evaluation of characteristic parameters for each diffusion mode based on the MSD-Δt plot have been developed (Figs. 6 and 7).

3. The procedure for determining motional modes and parameters is as follows. From the trajectory, a MSD-Δt plot is made and D_{2-4} is determined. If D_{2-4} is larger than 4.6×10^{-12} cm²/s, RD(1000, 90) is calculated and the motional mode is determined using Fig. 6 S. (If D_{2-4} is smaller than 4.6×10^{-12} cm²/s, the trajectory is classified as stationary mode.) v and L are determined by fitting the MSD-Δt plots using Eqs. 8 and 11, for directed and restricted diffusion, respectively.

4. We propose that the membrane-skeleton fence structure is a basic feature of the plasma membrane. The plasma membrane is divided into many small compartments with the diagonal lengths of 300–600 nm for the dif-

fusion of membrane proteins by the presence of the membrane-skeleton meshwork (Fig. 14). Some compartments are larger than 1 μm and were not detected by the present experimental design. The microscopic diffusion coefficient (D_{2-4}) within a compartment varies greatly, ranging between 4.6×10^{-12} and 1×10^{-9} cm²/s (Fig. 11). This model, which we refer to as the "membrane skeleton fence model," is an extension of the SPEQ gate model of the erythrocyte membrane (Tsuji et al., 1988) and agrees with our current knowledge of membrane skeletons (Bennett, 1990).

5. Calcium-induced differentiation strongly influenced E-cadherin motion on the dorsal/apical cell surface. The cytoskeleton/membrane-skeleton-bound component, which is the sum of the molecules exhibiting the directed diffusion and the stationary modes, includes ~60% of the particles in the low-calcium medium but only 8% in the high-calcium medium (Fig. 10). Therefore, the regulation mechanism specific to E-cadherin movements and assembly depends on the calcium-induced differentiation.

APPENDIX:
ANALYTICAL EXPRESSION OF MSD VERSUS ΔT FOR PARTICLES UNDERGOING RESTRICTED DIFFUSION CONFINED WITHIN REFLECTING BOUNDARIES

The general analytical expression of MSD versus Δt for restricted diffusion in both the presence and absence of a uniform drift velocity is presented here. Consider one-dimensional diffusion (Wiener process) confined between two reflecting boundaries at $x = 0$ and L. Let $P(y, t|x, 0)$ be a transition probability that the position of a particle is y at time t, given that it was x at $t = 0$. The diffusion equation is given by

$$\mathbf{L}_x[P(y, t|x, 0)] - \frac{\partial P(y, t|x, 0)}{\partial t} = 0$$

$$\mathbf{L}_y^*[P(y, t|x, 0)] - \frac{\partial P(y, t|x, 0)}{\partial t} = 0$$

$$\mathbf{L}_x = \mu \frac{\partial}{\partial x} + \frac{\sigma^2}{2} \frac{\partial^2}{\partial x^2} \tag{A1}$$

$$\mathbf{L}_y^* = -\mu \frac{\partial}{\partial y} + \frac{\sigma^2}{2} \frac{\partial^2}{\partial y^2}$$

$$\sigma^2 = 2D,$$

where D is the diffusion coefficient and μ is the drift velocity. The boundary conditions are

$$P(y, t) = \int_0^L P(y, t|x, 0)P(x, 0) \, dx$$

$$\mu P(y, t) - \frac{\sigma^2}{2} \frac{\partial P(y, t)}{\partial y} = 0 \qquad (y = 0, L), \tag{A2}$$

where $P(y, t)$ and $P(x, 0)$ are the distribution functions of the particle at times t and 0, respectively (Doob, 1953; Ogura, 1978).

Using the Laplace transform of $P(y, t|x, 0)$

$$G(y|x, \lambda) = \int_0^\infty P(y, t|x, 0)e^{\lambda t} dt \qquad (\text{Re } \lambda < 0), \tag{A3}$$

the diffusion equation (Eq. A1) and the boundary conditions (Eq. A2) can be transformed to

$$\mathbf{L}_x[G(y|x, \lambda)] + \lambda G(y|x, \lambda) = -\delta(x - y)$$

$$\mathbf{L}_y^*[G(y|x, \lambda)] + \lambda G(y|x, \lambda) = -\delta(x - y)$$

$$\frac{\partial G(y|x, \lambda)}{\partial x} = 0 \qquad (x = 0, L) \tag{A4}$$

$$\mu G(y|x, \lambda) - \frac{\sigma^2}{2} \frac{\partial G(y|x, \lambda)}{\partial y} = 0 \qquad (y = 0, L).$$

Here $G(y|x, \lambda)$ is a Green function on x and an adjoint Green function on y. In order to solve $G(y|x, \lambda)$, we introduce $u_0(x, \lambda)$, $u_L(x, \lambda)$, $v_0(y, \lambda)$, and $v_L(y, \lambda)$ that satisfy the differential equations

$$\mathbf{L}_x[u(x, \lambda)] + \lambda u(x, \lambda) = 0$$

$$\mathbf{L}_y^*[v(y, \lambda)] + \lambda v(y, \lambda) = 0. \tag{A5.1}$$

and the boundary conditions

$$\frac{\partial u(x, \lambda)}{\partial x} = 0 \qquad (x = 0, L)$$

$$\mu v(y, \lambda) - \frac{\sigma^2}{2} \frac{\partial v(y, \lambda)}{\partial y} = 0 \qquad (y = 0, L). \tag{A5.2}$$

$G(y|x, \lambda)$ is then given by

$$G(y|x, \lambda) = \begin{cases} \dfrac{v_L(y, \lambda)u_0(x, \lambda)}{J(\lambda)} & (0 < x < y < L) \\[2mm] \dfrac{v_0(y, \lambda)u_L(x, \lambda)}{J(\lambda)} & (0 < y < x < L) \end{cases}, \tag{A6.1}$$

where

$$J(\lambda) = \frac{1}{2} \exp\left(\frac{2\mu x}{\sigma^2}\right)[\dot{u}_0(x, \lambda)u_L(x, \lambda) - u_0(x, \lambda)\dot{u}_L(x, \lambda)] \tag{A6.2}$$

$$\dot{u} = \frac{du}{dx}.$$

This solution is proven by substitution to Eq. A4.

$P(y, t|x, 0)$ can be obtained by carrying out the inverse Laplace transformation of Eq. A3, that is,

$$P(y, t|x, 0) = \frac{1}{2\pi i} \int_{-i\infty + \epsilon}^{i\infty + \epsilon} G(y|x, \lambda)e^{-\lambda t}d\lambda \qquad (0 < \epsilon). \tag{A7}$$

This complex integral can be executed by Cauchy integral with a result of

$$P(y, t|x, 0) = q(y) + \frac{2}{L} \exp\left\{\frac{\mu}{\sigma^2}\left(y - x - \frac{\mu t}{2}\right)\right\}$$

$$\times \sum_{n=1}^{\infty} \frac{\varphi_n(x)\varphi_n(y)}{(n\pi\sigma/L)^2 + \mu^2/\sigma^2} \exp\left\{-\frac{1}{2}\left(\frac{n\pi\sigma}{L}\right)^2 t\right\} \quad (t > 0)$$

$$q(y) = \frac{2\mu}{\sigma^2} \exp\left(\frac{2\mu}{\sigma^2} y\right)\left[\exp\left(\frac{2\mu}{\sigma^2}L\right) - 1\right]^{-1} \tag{A8}$$

$$\varphi_n(x) = \frac{n\pi\sigma}{L} \cos\left(\frac{n\pi x}{L}\right) + \frac{\mu}{\sigma} \sin\left(\frac{n\pi x}{L}\right)$$

$$P(y, t|x, 0) = \delta(y - x) \qquad (t = 0),$$

where $q(y)$ is the probability density at the steady state.

In a particular case where the drift velocity $\mu = 0$, the expression reduces to

$$P(y, t|x, 0)$$

$$= \frac{1}{L} + \frac{2}{L} \sum_{n=1}^{\infty} \cos\left(\frac{n\pi x}{L}\right)\cos\left(\frac{n\pi y}{L}\right)\exp\left\{-\frac{1}{2}\left(\frac{n\pi\sigma}{L}\right)^2 t\right\} \quad (t > 0)$$

$$P(y, t|x, 0) = \delta(y - x) \qquad (t = 0). \tag{A9}$$

The steady-state distribution in this case is uniform between 0 and L. MSD can be calculated as

$$\langle x^2 \rangle(t) = \frac{\int_0^L \int_0^L (y - x)^2 P(y, t|x, 0)P(x, 0) \, dy \, dx}{\int_0^L P(x, 0) \, dx}. \tag{A10}$$

When the initial distribution of a particle is uniform in the interval between 0 and L, integration by terms yields

$$\langle x^2 \rangle(t) = \frac{L^2}{6} - \frac{16L^2}{\pi^4} \sum_{n=1 \text{(odd)}}^{\infty} \frac{1}{n^4} \exp\left\{-\frac{1}{2}\left(\frac{n\pi\sigma}{L}\right)^2 t\right\}, \tag{A11}$$

which is the expression used in this paper.

In the case where the drift velocity $\mu \neq 0$, and the initial distribution of a particle is uniform between 0 and L, MSD can be obtained as

$$\langle x^2 \rangle(t) = R(\mu, \sigma, L) - \sum_{n=1}^{\infty} \frac{8n^2\pi^2\mu\sigma^4}{L^3A_n(\mu, \sigma, L)^3B(\mu, \sigma, L)}$$

$$\times \exp\left(-\frac{A_n(\mu, \sigma, L)t}{2}\right)\left\{1 - \exp\left(\frac{\mu L}{\sigma^2}\right)\cos(n\pi)\right\}^2$$

$$R(\mu, \sigma, L) = \frac{\sigma^4}{2\mu^2} - \frac{2L^2}{B(\mu, \sigma, L)^2}\exp\left(\frac{2\mu L}{\sigma^2}\right) \tag{A12}$$

$$A_n(\mu, \sigma, L) = \frac{\mu^2}{\sigma^2} + \frac{n^2\pi^2\sigma^2}{L^2}$$

$$B(\mu, \sigma, L) = \exp\left(\frac{2\mu L}{\sigma^2}\right) - 1.$$

REFERENCES

Abney, J. R., B. A. Scalettar, and J. C. Owicki. 1989. Self diffusion of interacting membrane proteins. *Biophys. J.* 55:817–833.

Anderson, C. M., G. N. Georgiou, I. E. G. Morrison, G. V. Stevenson, and R. J. Cherry. 1992. Tracking of cell surface receptors by fluorescence digital imaging microscopy using a charge-coupled device camera. Low-density lipoprotein and influenza virus receptor mobility at 4°C. *J. Cell Sci.* 101:415–425.

Austin, R. A., S. S. Chan, and T. Jovin. 1979. Rotational diffusion of cell surface components by time-resolved phosphorescence anisotropy. *Proc. Natl. Acad. Sci. USA.* 76:5650–5654.

Axelrod, D., D. E. Koppel, J. Schlessinger, E. L. Elson, and W. W. Webb. 1976. Mobility measurements by analysis of fluorescence photobleaching recovery kinetics. *Biophys. J.* 16:1055–1069.

Bennett, V. 1990. Spectrin-based membrane skeleton: a multipotential adaptor between plasma membrane and cytoplasm. *Physiol. Rev.* 70:1029–1065.

Chang, C. H., H. Takeuchi, T. Ito, K. Machida, and S. Ohnishi. 1981. Lateral mobility of erythrocyte membrane proteins studied by the fluorescence photobleaching recovery technique. *J. Biochem.* 90:997–1004.

Cherry, R. J., A. Bürkli, M. Busslinger, G. Schneider, and G. R. Parish. 1976. Rotational diffusion of band 3 proteins in the human erythrocyte membrane. *Nature (Lond.).* 263:389–393.

Cherry, R. J. 1979. Rotational and lateral diffusion of membrane proteins. *Biochim. Biophys. Acta.* 559:289–327.

Cherry, R. J. 1992. Keeping track of cell surface receptors. *Trends Cell Biol.* 2:242–244.

De Brabander, M., G. Geuens, R. Nuydens, M. Moeremans, and J. de Mey. 1985. Probing microtubule-dependent intracellular motility with nanometre particle video ultramicroscopy (nanovid ultramicroscopy). *Cytobios.* 43:273–283.

De Brabander, M., R. Nuydens, G. Geuens, M. Moeremans, and J. de Mey. 1986. The use of submicroscopic gold particles combined with video contrast enhancement as a simple molecular probe for the living cell. *Cell Motil. Cytoskeleton.* 6:105–113.

De Brabander, M., R. Nuydens, H. Geerts, and C. R. Hopkins. 1988. Dynamic behavior of the transferrin receptor followed in living epidermoid carcinoma (A431) cells with nanovid microscopy. *Cell Motil. Cytoskeleton.* 9:30–47.

De Brabander, M., R. Nuydens, A. Ishihara, B. Holifield, K. Jacobson, and H. Geerts. 1991. Lateral diffusion and retrograde movements of individual cell surface components on single motile cells observed with nanovid microscopy. *J. Cell Biol.* 112:111–124.

De Mey, J. R. 1983. Colloidal gold probes in immunocytochemistry. *In* Immunochemistry. Practical Applications in Pathology and Biology. J. M. Polak and S. van Noorden, editors. Wright PSG, Bristol, U.K. 82–111.

den Hartigh, J. C., P. M. P. van Bergen en Henegouwen, A. J. Verkleij, and J. Boonstra. 1992. The EGF receptor is an actin binding protein. *J. Cell Biol.* 119:349–355.

Doob, J. L. 1953. Stochastic Processes. Wiley, New York.

Dubinsky, J. M., D. J. Loftus, G. D. Fischbach, and E. L. Elson. 1989. Formation of acetylcholine receptor clusters in chick myotubes: migration or new insertion? *J. Cell Biol.* 109:1733–1743.

Edidin, M. 1987. Rotational and lateral diffusion of membrane proteins and lipids: phenomena and function. *Curr. Top. Membr. Transp.* 29:91–127.

Edidin, M. 1990. Molecular associations and membrane domains. *Curr. Top. Membr. Transp.* 36:81–96.

Edidin, M., and I. Stroynowski. 1991. Differences between the lateral organization of conventional and inositol phospholipid anchored membrane proteins. A further definition of micrometer scale membrane domains. *J. Cell Biol.* 112:1143–1150.

Edidin, M., S. C. Kuo, and M. P. Sheetz. 1991. Lateral movements of membrane glycoproteins restricted by dynamic cytoplasmic barriers. *Science (Washington DC).* 254:1379–1382.

Elson, E. L. 1985. Fluorescence correlation spectroscopy and photobleaching recovery. *Annu. Rev. Phys. Chem.* 36:379–406.

Geerts, H., M. De Brabander, R. Nuydens, G. Geuens, M. Moeremans, J. de Mey, and P. Hollenbeck. 1987. Nanovid tracking: a new automatic method for the study of mobility in living cells based on colloidal gold and video microscopy. *Biophys. J.* 52:775–782.

Geerts, H., M. de Brabander, and R. Nuydens. 1991. Nanovid microscopy. *Nature (Lond.).* 351:765–766.

Gelles, J., Schnapp, B. J., and M. P. Sheetz. 1988. Tracking kinesin-driven movements with nanometer-scale precision. *Nature (Lond.).* 331: 450–453.

Goldstein, J. L., M. S. Brown, R. G. W. Anderson, D. W. Russell, and W. J. Schneider. 1985. Receptor-mediated endocytosis: concepts emerging from the LDL receptor system. *Annu. Rev. Cell Biol.* 1:1–39.

Ghosh, R. N., and W. W. Webb. 1990. Evidence for intra-membrane constraints to cell surface LDL receptor motion. *Biophys. J.* 57:286a. (Abstr.)

Gross, D. J., and W. W. Webb. 1988. Cell surface clustering and mobility of the liganded LDL receptor measured by digital video fluorescence microscopy. *In* Spectroscopic Membrane Probes II. L. M. Loew, editor. CRC Press, Boca Raton, FL. 19–45.

Hennings, H., M. D. Cheng, P. Steinert, K. S. Holbrook, and S. H. Yuspa. 1980. Calcium regulation of growth and differentiation of mouse epidermal cells in culture. *Cell.* 19:245–254.

Hennings, H., F. H. Kurszewski, S. H. Yuspa, and R. W. Tucker. 1989. Intercellular calcium alterations in response to increased external calcium in normal and neoplastic keratinocytes. *Carcinogenesis (Lond.).* 10: 777–780.

Hillman, G. M., and J. Schlessinger. 1982. The lateral diffusion of epidermal growth factor complexed to its surface receptors does not account for the thermal sensitivity of patch formation and endocytosis. *Biochemistry.* 21:1667–1672.

Hirano, S., A. Nose, K. Hatta, A. Kawakami, and M. Takeichi. 1987. Calcium-dependent cell-cell adhesion molecules (cadherins): subclass specificities and possible involvement of actin bundles. *J. Cell Biol.* 105: 2501–2510.

Hyde, J. S., and L. Dalton. 1972. Very slowly tumbling spin labels: adiabatic rapid passage. *Chem. Phys. Lett.* 16:568–572.

Iacopetta, B. J., S. Rathanberger, and L. C. Kühn. 1988. A role for the cytoplasmic domain in transferrin receptor sorting and coated pit formation during endocytosis. *Cell.* 54:485–489.

Jacobson, K., A. Ishihara, and R. Inman. 1987. Lateral diffusion of proteins in membranes. *Annu. Rev. Physiol.* 49:163–175.

Johnson, P., and P. Garland. 1981. Depolarization of fluorescence depletion. A microscopic method for measuring rotational diffusion of membrane proteins on the surface of a single cell. *FEBS Lett.* 132:252–256.

Kemler, R., and M. Ozawa. 1989. Uvomorulin-catenin complex: cytoplasmic anchorage of a Ca^{2+}-dependent cell adhesion molecule. *Bioessays.* 11:88–91.

Kucik, D. F., E. L. Elson, and M. P. Sheetz. 1989. Forward transport of glycoproteins on leading lamellipodia in locomoting cells. *Nature (Lond.).* 340:315–317.

Kulesz-Martin, M., A. E. Kilkenny, K. A. Holbrook, V. Digernes, and S. H. Yuspa. 1983. Properties of carcinogen altered mouse epidermal cells resistant to calcium-induced terminal differentiation. *Carcinogenesis (Lond.).* 4:1367–1377.

Kusumi, A., S. Ohnishi, T. Ito, and T. Yoshizawa. 1978. Rotational motion of rhodopsin in the visual receptor membrane as studied by saturation transfer spectroscopy. *Biochim. Biophys. Acta.* 507:539–543.

Kusumi, A., T. Sakaki, T. Yoshizawa, and S. Ohnishi. 1980. Protein-lipid interaction in rhodopsin recombinant membranes as studied by protein rotational mobility and lipid alkyl chain flexibility measurements. *J. Biochem.* 88:1103–1111.

Kusumi, A., and J. S. Hyde 1982. Spin-label saturation transfer electron spin resonance detection of transient association of rhodopsin in reconstituted membranes. *Biochemistry.* 21:5978–5983.

Kusumi, A., W. K. Subczynski, M. Pasenkiewicz-Gierula, J. S. Hyde, and H. Merkle. 1986. Spin-label studies on phosphatidylcholine-cholesterol membranes: effects of alkyl chain length and unsaturation in the fluid phase. *Biochim. Biophys. Acta.* 854:307–317.

Kusumi, A., A. Tsuji, M. Murata, Y. Sako, S. Kagiwada, T. Hayakawa, and S. Ohnishi. 1990. Development of time-resolved microfluorimetry and its application to studies of cellular membranes. SPIE Proc. 1204. *In* Time-Resolved Laser Spectroscopy in Biochemistry II. J. R. Lakowicz, editor. SPIE Press, Bellingham, WA.

Landreth, G. E., L. K. Williams, and G. D. Reiser. 1985. Association of the epidermal growth factor receptor kinase with the detergent-insoluble cytoskeleton of A431 cells. *J. Cell Biol.* 101:1341–1350.

Lee, G. M., A. Ishihara, and K. A. Jacobson. 1991. Direct observation of Brownian motion of lipids in a membrane. *Proc. Natl. Acad. Sci. USA.* 88:6274–6278.

Leunissen, J. L. M., and de Mey, J. R. 1986. Preparation of gold probes. *In* Immuno-gold Labeling Cell Biology. A. J. Verkleij and J. L. M. Leunissen, editors. CRC Press, Boca Raton, FL. 3–16.

Livneh, E., M. Benveniste, R. Prywes, S. Felder, Z. Kam, and J. Schlessinger. 1986. Large deletions in the cytoplasmic kinase domain of the epidermal growth factor receptor do not affect its lateral mobility. *J. Cell Biol.* 103:327–331.

McCrea, P. D., and B. M. Gumbiner. 1991. Purification of a 92-kDa cytoplasmic protein tightly associated with the cell-cell adhesion molecule E-cadherin (uvomorulin). Characterization and extractability of the protein complex from the cell cytostructure. *J. Biol. Chem.* 266:4514–4520.

McNeill, H., M. Ozawa, R. Kemler, and W. J. Nelson. 1990. Novel function of the cell adhesion molecule uvomorulin as an inducer of cell surface polarity. *Cell.* 62:309–316.

Mecham, R. M., L. Whitehouse, M. Hay, A. Hinek, and M. P. Sheetz. 1991. Ligand affinity of the 67-kD elastin/laminin binding protein is modulated by the protein's lectin domain: visualization of elastin/laminin-receptor complexes with gold-tagged ligands. *J. Cell Biol.* 113:187–194.

Metzger, H. 1992. Transmembrane signaling. The joy of aggregation. *J. Immunol.* 149:1477–1487.

Miller, K., M. Shipman, I. S. Trowbridge, and C. R. Hopkins. 1991. Transferrin receptors promote the formation of clathrin lattices. *Cell.* 65: 621–632.

Moore, C., D. Boxer, and P. Garland. 1979. Phosphorescence depolarization and the measurement of rotational motion of proteins in membranes. *FEBS Lett.* 108:161–166.

Nagafuchi, A., and M. Takeichi. 1988. Cell binding function of E-cadherin is regulated by the cytoplasmic domain. *EMBO J.* 7:3679–3684.

Nagafuchi, A., Y. Shirayoshi, K. Okazaki, K. Yasuda, and M. Takeichi. 1987. Transformation of cell adhesion properties by exogenously introduced E-cadherin cDNA. *Nature (Lond.).* 329:341–343.

Ogura, H. 1978. Stochastic Processes. Corona Press, Tokyo.

Ozawa, M., H. Baribault, and R. Kemler. 1989. The cytoplasmic domain of the cell adhesion molecules uvomorulin associates with three independent proteins structurally related in different species. *EMBO J.* 8:1711–1717.

Ozawa, M., M. Ringwald, and R. Kemler. 1990. Uvomorulin-catenin complex formation is regulated by a specific domain in the cytoplasmic region of the cell adhesion molecule. *Proc. Natl. Acad. Sci. USA.* 87:4246–4250.

Peters, R., and R. J. Cherry. 1982. Lateral and rotational diffusion of bacteriorhodopsin in lipid bilayers: experimental test of the Saffman-Delbrück equations. *Proc. Natl. Acad. Sci. USA.* 79:4317–4321.

Qian, H., M. P. Sheetz, and E. L. Elson. 1991. Single particle tracking. Analysis of diffusion and flow in two-dimensional systems. *Biophys. J.* 60:910–921.

Ryan, T. A., J. Myers, D. Holowka, B. Baird, and W. W. Webb. 1988. Molecular crowding on the cell surface. *Science (Washington DC).* 239: 61–64.

Saffman, P. G., and M. Delbrück. 1975. Brownian motion in biological membranes. *Proc. Natl. Acad. Sci. USA.* 72:3111–3115.

Saxton, M. J. 1982. Lateral diffusion in archipelago: effects of impermeable patches on diffusion in a cell membrane. *Biophys. J.* 39:165–173.

Saxton, M. J. 1987. Lateral diffusion in archipelago. The effect of mobile obstacles. *Biophys. J.* 52:989–997.

Saxton, M. J. 1989a. Lateral diffusion in archipelago. Distance dependence of the diffusion coefficient. *Biophys. J.* 56:615–622.

Saxton, M. J. 1989b. The spectrin network as a barrier to lateral diffusion in erythrocytes. A percolation analysis. *Biophys. J.* 55:21–28.

Saxton, M. J. 1990. The membrane skeleton of erythrocytes. A percolation model. *Biophys. J.* 57:1167–1177.

Saxton, M. J. 1991. The membrane skeleton of erythrocytes: models and its effect on lateral diffusion. *Int. J. Biochem.* 22:801–809.

Saxton, M. J. 1992. Lateral diffusion and aggregation. A Monte Carlo study. *Biophys. J.* 61:119–128.

Saxton, M. J. 1993. Lateral diffusion in an archipelago. Single-particle diffusion. *Biophys. J.* 64:1766–1780.

Schlessinger, J. 1986. Allosteric regulation of the epidermal growth factor receptor kinase. *J. Cell Biol.* 103:2067–2072.

Schlessinger, J., A. B. Schreiber, A. Levi, I. Lax, T. Liberman, and Y. Yarden. 1983. Regulation of cell proliferation by epidermal growth factor. *CRC Crit. Rev. Biochem.* 14:93–111.

Schnapp, B. J., J. Gelles, and M. P. Sheetz. 1988. Nanometer-scale measurement using video light microscopy. *Cell Motil. Cytoskeleton.* 10:47–53.

Sheetz, M. P. 1993. Glycoprotein motility and dynamic domains in fluid plasma membranes. *Annu. Rev. Biophys. Biomol. Struct.* 22:417–431.

Sheetz, M. P., M. Schindler, and D. E. Koppel. 1980. Lateral mobility of integral membrane proteins is increased in spherocyte erythrocytes. *Nature (Lond.).* 285:510–512.

Sheetz, M. P., S. Turney, H. Qian, and E. L. Elson. 1989. Nanometre-level analysis demonstrates that lipid flow does not drive membrane glycoprotein movements. *Nature (Lond.).* 340:284–288.

Sheetz, M. P., N. L. Baumrind, D. B. Wayne, and A. L. Pearlman. 1990. Concentration of membrane antigens by forward transport and trapping in neuronal growth cones. *Cell.* 61:231–241.

Takeichi, M. 1988. The cadherins: cell-cell adhesion molecules controlling animal morphogenesis. *Development (Camb.).* 102:639–655.

Thomas, D. D., L. R. Dalton, and J. S. Hyde. 1976. Rotational diffusion studied by passage saturation transfer electron paramagnetic resonance. *J. Chem. Phys.* 65:3006–3024.

Tsuji, A., K. Kawasaki, S. Ohnishi, H. Merkle, and A. Kusumi. 1988. Regulation of band 3 mobilities in erythrocyte ghost membranes by protein association and cytoskeletal meshwork. *Biochemistry.* 27:7447–7452.

Tsuji, A., and S. Ohnishi. 1986. Restriction of the lateral motion of band 3 in the erythrocyte membrane by the cytoskeletal network: dependence on spectrin association state. *Biochemistry.* 25:6133–6139.

van Beijeren, H., and R. Kutner. 1985. Mean square displacement of a tracer particle in a hard-core lattice gas. *Phys. Rev. Lett.* 55:238–241.

Vaz, W. L. C., F. Goodsaid-Zalduondo, and K. Jacobson. 1984. Lateral diffusion of lipids and proteins in bilayer membranes. *FEBS Lett.* 174: 199–207.

Vaz, W. L. C., E. C. C. Melo, and T. E. Thompson. 1989. Translational diffusion and fluid domain connectivity in a two-component, two-phase phospholipid bilayer. *Biophys. J.* 56:869–876.

Wiegant, F. A. C., F. J. Blok, L. H. K. Defize, W. A. M. Linnemans, A. J. Verkleij, and J. Boonstra. 1986. Epidermal growth factor receptors associated to cytoskeletal elements of epidermoid carcinoma (A431) cells. *J. Cell Biol.* 103:87–94.

Yoshitake, S., M. Imagawa, E. Ishikawa, Y. Niitsu, I. Urushizaki, M. Nishiura, R. Kanazawa, H. Kurosaki, S. Tachibana, N. Nakazawa, and H. Ogawa. 1982. Mild and efficient conjugation of rabbit Fab' and horseradish peroxidase using a maleimide compound and its use for enzyme immunoassay. *J. Biochem.* 92:1413–1412.

Yuspa, S. H., and D. L. Morgan. 1981. Mouse skin cells resistant to terminal differentiation associated with initiation of carcinogenesis. *Nature (Lond.).* 293:72–74.

Zhang, F., B. Crise, B. Su, Y. Hou, J. K. Rose, A. Bothwell, and K. Jacobson. 1991. Lateral diffusion of membrane-spanning and glycosyl-phosphatidylinositol-linked proteins: toward establishing rules governing the lateral mobility of membrane proteins. *J. Cell Biol.* 115:75–84.

Zidovetzki, R., M. Bartholdi, D. Arndt-Jovin, and T. M. Jovin. 1986. Rotational dynamics of the Fc receptor for immunoglobulin E on histamine-releasing rat basophilic leukemia cells. *Biochemistry.* 25:4397–4401.